2.5 Geology, Seismology, and Geotechnical Engineering

NAPS COL 2.0-26-A
NAPS COL 2.0-27-A
NAPS COL 2.0-28-A
NAPS COL 2.0-29-A
NAPS COL 2.0-30-A

The information needed to address DCD COL Items 2.0-26-A, 2.0-27-A, 2.0-28-A, 2.0-29-A, and 2.0-30-A are included in SSAR Section 2.5, which is incorporated by reference with the following variance and supplements. Vertical datum is with reference to NAVD88 throughout Section 2.5, unless stated otherwise.

The first two paragraphs of SSAR Section 2.5 are replaced as follows.

NAPS ESP VAR 2.0-4

This section presents information on the geological, seismological, and geotechnical engineering properties of the Unit 3 site and the region surrounding the site. Section 2.5.1 describes basic geological and seismologic data based on those data developed since publication of the EPRI 1986 seismic source model (SSAR Reference 1) with additional information based on the Central and Eastern United States Seismic Source Characterization (CEUS SSC) for Nuclear Facilities Project (Reference 2.5-223) and the moment magnitude (**M**) 5.8 earthquake that occurred near Mineral, Louisa County, VA on August 23, 2011. Section 2.5.2 describes the vibratory ground motion at the site, the CEUS SSC model as documented in NUREG-2115 (Reference 2.5-223), and an update of the seismicity catalog. The CEUS SSC model, which incorporates the Electric Power Research Institute (EPRI) ground motion prediction equations (GMPEs) (References 2.5-224 and 2.5-225), is used to perform a hard rock probabilistic seismic hazard analysis (PSHA) and develop uniform hazard response spectra (UHRS). Site-specific strong ground motion amplification factors are developed using properties of subsurface materials described in Section 2.5.4. These amplification factors and the hard rock UHRS are combined to define the ground motion response spectra (GMRS) following the guidance in RG 1.208, A Performance-Based Approach to Define the Site-Specific Earthquake Ground Motion (Reference 2.5-226). Section 2.5.3 describes the potential for surface faulting in the site area, and Sections 2.5.4, 2.5.5, and 2.5.6 describe the stability of surface materials and foundations at the site.

RG 1.208, Appendix C, “Investigations to Characterize Site Geology, Seismology and Geophysics” (Reference 2.5-226), provides guidance for the level of investigation recommended at different distances from a proposed site for a nuclear facility. The site region is that area within

200 miles (320 km) of the site location. The site vicinity is that area within 25 miles (40 km) of the site location. The site area is that area within 5 miles (8 km) of the site location. The site is that area within 0.6 mile (1 km) of the site location. These terms, site region, site vicinity, site area, and site, are used in Sections 2.5.1 through 2.5.3 to describe these specific areas of investigation. These terms are not applicable to other sections of the FSAR.

2.5.1 Basic Geologic and Seismic Information

NAPS COL 2.0-26-A

The information needed to address DCD COL Item 2.0-26-A is included in SSAR Section 2.5.1, which is incorporated by reference with the following variance and supplements.

The first three paragraphs of SSAR Section 2.5.1 are replaced as follows.

NAPS ESP VAR 2.0-4

This section presents information on the geological and seismological characteristics of the Unit 3 site region and area. The information is divided into two parts. SSAR Section 2.5.1.1 describes the geologic and tectonic setting of the site region and SSAR Section 2.5.1.2 describes the geology and structural geology of the site area. The geological and seismological information was developed in accordance with the guidance presented in RG 1.70, Section 2.5.1, “Basic Geologic and Seismic Information” (SSAR Reference 3), RG 1.206, “Combined License Applications for Nuclear Power Plants” (Reference 2.5-203), and RG 1.208. This information is intended to satisfy the requirements of 10 CFR 100, “Reactor Site Criteria,” Section 100.23, “Geologic and Seismic Siting Criteria,” paragraph (c) “Geological, Seismological and Engineering Characteristics” (SSAR Reference 4). The geological and seismological information presented in this section are used as a basis for evaluating the geologic, seismic, and man-made hazards at the site.

RG 1.208 states that seismic sources identified and characterized by EPRI (References 2.5-227 and 2.5-228) and Lawrence Livermore National Laboratory (LLNL) (References 2.5-229, 2.5-230, and 2.5-231) are to be used for studies in the CEUS. However, the EPRI-SOG model and the LLNL model were replaced by the CEUS SSC model and database (Reference 2.5-223).

The geological and seismological information presented in this section was developed from a review of previous reports prepared for existing

Units 1 and 2 and the abandoned Units 3 and 4, published geologic literature, interpretation of aerial photography, subsurface investigations, and field and aerial reconnaissance. Previous site-specific reports reviewed include the existing Units 1 and 2 UFSAR (SSAR Reference 5) and ISFSI Safety Analysis Report (SSAR Reference 6). Reports prepared by Dames and Moore for design and construction of the existing units (SSAR Reference 7) and the abandoned Units 3 and 4 (SSAR References 8 and 9) were also reviewed. A review of published geologic literature was used to supplement and update the existing geological and seismological information. This literature was identified using the GeoRef database (American Geological Institute) and the USGS library catalogue. In addition, relevant unpublished geologic literature, studies, and projects were identified by contacting the USGS, State geological survey organizations, and universities. This section includes information on the **M** 5.8 earthquake that occurred on August 23, 2011 in Mineral, Louisa County, Virginia, and the results of a geological reconnaissance to investigate any surface features associated with the earthquake in the site vicinity. A list of the references used to compile the geological and seismological information presented in the following sections is provided at the end of Section 2.5.

2.5.1.1.4 Regional Tectonic Setting

The first two paragraphs of SSAR Section 2.5.1.1.4 are replaced as follows.

NAPS ESP VAR 2.0-4

The CEUS SSC Project was conducted by EPRI, the DOE, and the NRC from April 2008 to December 2011. The purpose of this project was to provide a regional seismic source model for use in the PSHA for a nuclear facility in the CEUS. This study replaces regional seismic source models developed for performing a PSHA including the EPRI-SOG model and the LLNL model. The CEUS SSC model is described in detail in Reference 2.5-223.

The following four sections (a-d) describe the site region in terms of plate tectonic evolution, origin and orientation of tectonic stress, primary tectonic features, and previously-defined seismic sources. Figure 2.5.1-202 provides an overview of the eastern United States and the seismotectonic zones from the CEUS SSC. The CEUS SSC host source for the Unit 3 site is the Extended Continental Crust-Atlantic Margin Zone (ECC-AM) defined to include the region characterized by

the presence of extended continental crust developed during Mesozoic rifting along the Atlantic Ocean basin margin (Reference 2.5-223). The ECC-AM and the source immediately to the west, the Paleozoic Extended Crust Zone (PEZ) are characterized by the geologic structures described below. The Atlantic Highly Extended Crust Zone (AHEX) is located to the east of the ECC-AM and represents the region of highly extended crust that is the transition between the extended, thick continental crust of the ECC-AM and the thinner mafic oceanic crust (Atlantic Ocean basin). Historical seismicity occurring in the site region is described in Section 2.5.2.1. The CEUS SSC methodology and seismic sources relevant to the Unit 3 site are described in greater detail in Sections 2.5.2.2.3 and 2.5.2.3.

a. **Plate Tectonic Evolution of the Appalachian Orogenic Belt at the Latitude of the Site Region**

The first sentence of the third paragraph of Item a of this SSAR section is replaced as follows.

NAPS ESP VAR 2.0-4

SSAR Figure 2.5-6 is a simplified tectonic map showing the five onshore physiographic provinces of Virginia and the belts and terranes within the Blue Ridge and Piedmont Provinces, as delineated by Hatcher (SSAR Reference 45) and Horton and others (SSAR Reference 46).

The second sentence of the eighth paragraph of Item a of this SSAR section is replaced as follows.

NAPS ESP VAR 2.0-4

This model represents a significant alternative interpretation of the origin and affinity of the crust east of the Spotsylvania thrust fault in the region of the Unit 3 site.

b. **Tectonic Stress in the Mid-Continent Region**

NAPS ESP VAR 2.0-4

The last paragraph of Item b of this SSAR section is replaced as follows.

Data that post-date the World Stress Map (SSAR References 50, 51, and 52) suggest that the local stress field in the central Virginia area may deviate from the overall regional orientation. For example, studies by Mazzotti and Townend (2010) (Reference 2.5-391) and Hurd and Zoback (2012) (Reference 2.5-390) suggest that the orientation of the maximum horizontal compressive stress in the central Virginia area is approximately E-W.

Mazzotti and Townend (2010) use a Bayesian analysis of earthquake focal mechanisms to determine the state of stress in ten seismic zones in central and eastern North America and compare their results with those from shallower borehole measurements. For the Central Virginia Seismic Zone (CVSZ), their analysis is based on a total of thirteen earthquakes, including eleven small (M<3) earthquakes and two earthquakes with M approximately 4. For the CVSZ, Mazzotti and Townend (2010) report the maximum horizontal compressive stress is oriented approximately E-W, which is rotated approximately 48 degrees clockwise with respect to the regional trend obtained from shallower borehole data.

Hurd and Zoback (2012) present regional stress orientations for central and eastern North America based on 75 earthquake focal mechanisms and ten stress inversions. They report the regional stress field is generally characterized by an overall NE-SW orientation of the maximum horizontal compressive stress and that this orientation is remarkably consistent on the lateral scale of hundreds of kilometers. Similar to Mazzotti and Townend (2010), however, Hurd and Zoback (2012) report an approximately E-W orientation of the maximum horizontal compressive stress for a localized area in central Virginia. Taken together, Mazzotti and Townend (2010) and Hurd and Zoback (2012) suggest that the E-W-oriented stress field in the central Virginia area deviates from the large scale, regional NE-SW orientation.

The stress orientation data presented in Mazzotti and Townend (2010) and Hurd and Zoback (2012) predate the **M** 5.8 Mineral, Virginia earthquake of August 23, 2011. Aftershock data suggest a rupture plane that is oriented approximately NNE with a moderate dip to the ESE (e.g., Horton et al., 2012 (Reference 2.5-232); Chapman, 2012 (Reference 2.5-235); Horton, 2014 (Reference 2.5-393)). This earthquake is described in greater detail in Section 2.5.1.1.7. According to McNamara et al. (2014), the locations and focal mechanisms from the Mineral earthquake main event and numerous aftershocks indicate a rupture plane that strikes approximately N36° E and dips approximately 49.5° ESE, slightly oblique to the regional structural grain. The focal mechanism solutions presented by McNamara et al. (2014) for the Mineral earthquake main event and aftershocks principally are reverse-slip. As such, the Mineral earthquake rupture orientation and sense of motion are more consistent with the approximately E-W horizontal compressive stress orientation suggested by Mazzotti and

Townend (2010) and Hurd and Zoback (2012) for the local central Virginia area than for the regional NE-SW stress orientation.

If the local stress orientation of central Virginia is approximately E-W as indicated by Mazzotti and Townend (2010) and Hurd and Zoback (2012), as opposed to the approximately NE-SW orientation reported by the World Stress Map (SSAR References 50, 51, and 52), this suggests a more favorable orientation of maximum horizontal stress for reactivating structures that are approximately aligned with the NE-SW-oriented regional structural grain. This includes the fault that ruptured during the Mineral earthquake and other faults proximal to the site vicinity.

c. Principal Tectonic Structures

1. Paleozoic Tectonic Structures

The last sentence of the third paragraph of Item 1 under Item c of this SSAR section is replaced as follows.

NAPS ESP VAR 2.0-4

Therefore, these Paleozoic structures in the site region are not considered to be capable tectonic sources, as defined in RG 1.208, Appendix A.

The last sentence of the fourth paragraph of Item 1 under Item c of this SSAR section is replaced as follows.

NAPS ESP VAR 2.0-4

None of the faults located within 25 miles of the site are considered to be capable tectonic sources, as defined in RG 1.208, Appendix A.

NAPS ESP VAR 2.0-4

The last paragraph of Item 1 under Item c of this SSAR section is deleted.

2. Mesozoic Tectonic Structures

The first sentence of the first paragraph of Item 2 under Item c of this SSAR section is replaced as follows.

NAPS ESP VAR 2.0-4

Mesozoic basins have long been considered potential sources for earthquakes along the eastern seaboard and are considered to be characteristic of the ECC-AM Zone which is described in the CEUS SSC (Reference 2.5-223).

The first sentence of the second paragraph of Item 2 under Item c of this SSAR section is corrected as follows.

NAPS COR

Generally, the exposed rift basins are asymmetric half-grabens (SSAR Figure 2.5-9) with the primary rift-bounding faults on the western margin of the half-grabens.

The last paragraph of Item 2 under Item c of this SSAR section is replaced as follows.

NAPS ESP VAR 2.0-4

Crone and Wheeler (SSAR Reference 59) do not recognize any basin-margin faults that have been reactivated during the Quaternary in the site region. No Mesozoic basin in the site region is associated with a known capable tectonic source. Seismicity potentially associated with reactivation of faults bordering or beneath the Mesozoic basins is addressed in the CEUS SSC model (Reference 2.5-223).

3. Tertiary Tectonic Structures

The last paragraph under **Stafford Fault System** of Item 3 under Item c of this SSAR section is replaced as follows.

NAPS ESP VAR 2.0-4

The Stafford fault system is located within the ECC-AM (Reference 2.5-223). Field and aerial reconnaissance did not reveal any geologic or geomorphic features indicative of potential Quaternary activity along the fault system. Similarly, Crone and Wheeler (SSAR Reference 59) do not show the Stafford fault system as a Quaternary structure in their compilation of active tectonic features in the CEUS. The Stafford fault system, therefore, is not a capable tectonic source.

4. Quaternary Tectonic Features

A paragraph is added to the end of Item 4 under Item c of this SSAR section as follows.

NAPS ESP VAR 2.0-4

Aftershock data associated with the August 23, 2011, **M** 5.8 Mineral earthquake have been interpreted as a previously unmapped geologic structure, which Horton et al. (Reference 2.5-223) has termed the “Quail fault.” The “Quail fault” is a seismogenic structure (described in Section 2.5.1.1.7). Information on the Mineral earthquake is provided in Section 2.5.2. This structure does not fit the criteria for a repeated

large-magnitude earthquake (RLME) source as defined in Reference 2.5-223. See Section 2.5.2.2.5.1.

The last two sentences of the second paragraph under **Paleo-Liquefaction Features within the Central Virginia Seismic Zone** of Item 4 under Item c of this SSAR section are replaced as follows.

NAPS ESP VAR 2.0-4

These paleo-liquefaction features do not fit the criteria for RLME sources and are considered within the ECC-AM source zone in the CEUS SSC model (Reference 2.5-223).

The last sentence of the sixth paragraph under **Mountain Run Fault Zone** of Item 4 under Item c of this SSAR section is replaced as follows.

NAPS ESP VAR 2.0-4

It is concluded that the Mountain Run fault zone is not a capable tectonic source. The Evarona-Mountain Run fault zone is not defined as an RLME source and is considered within the ECC-AM seismic source zone in the CEUS SSC model (Reference 2.5-223).

NAPS ESP VAR 2.0-4

The last sentence of the second paragraph and the third paragraph under **East Coast Fault System** of Item 4 under Item c of this SSAR section are deleted.

The first and second sentences of the fourth paragraph under **East Coast Fault System** of Item 4 under Item c of this SSAR section are replaced as follows.

NAPS ESP VAR 2.0-4

The southern segment of the East Coast Fault System (ECFS) is in essence covered by the different Charleston source zone geometries.

NAPS ESP VAR 2.0-4

The fourth and fifth sentences of the fifth paragraph under **East Coast Fault System** of Item 4 under Item c of this SSAR section are deleted.

The third and fourth sentences of the sixth paragraph under **East Coast Fault System** of Item 4 under Item c of this SSAR section are replaced as follows.

NAPS ESP VAR 2.0-4

Geomorphic analyses and aerial reconnaissance indicate that the northern segment of the fault zone probably does not exist or has a very low probability of activity if it does exist. The ECFS is not defined as an

RLME source and is considered within the ECC-AM seismic source zone in the CEUS SSC model (Reference 2.5-223).

d. Seismic Sources Defined by Regional Seismicity

The first sentence of the first paragraph of Item d of this SSAR section is replaced as follows.

NAPS ESP VAR 2.0-4

Within 200 miles of the Unit 3 site, two previously recognized seismic sources are defined by a concentration of small to moderate earthquakes.

1. Central Virginia Seismic Zone

The last three sentences of the first paragraph of Item 1 under Item d of this SSAR section are deleted.

The fourth paragraph of Item 1 under Item d of this SSAR section is replaced as follows.

NAPS ESP VAR 2.0-4

Upper-bound maximum values of M_{max} used by the EPRI teams range from m_b 6.6 to 7.2 (SSAR Reference 1). Bollinger (SSAR Reference 79) estimated an M_{max} of m_b 6.4 for the Central Virginia seismic source. Chapman and Krimgold (SSAR Reference 57) have used an M_{max} of m_b 7.25 for the Central Virginia seismic source and most other sources in their seismic hazard analysis of Virginia.

However, new data and information on seismicity and seismic sources in the CEUS have led to the development of the CEUS SSC model. The Central Virginia Seismic Zone (CVSZ) is located within and comprises a portion of the ECC-AM Zone as defined by the CEUS SSC Project (Reference 2.5-223).

The August 23, 2011 earthquake has been referred to as both the Mineral, Virginia earthquake (References 2.5-233 and 2.5-234) and the Louisa County, Virginia earthquake (Reference 2.5-235). In the descriptions that follow, the term Mineral earthquake is used. The magnitude of the mainshock has been reported as both **M** 5.8 (References 2.5-233, 2.5-236, 2.5-237, 2.5-238, 2.5-239, and 2.5-240) and **M** 5.7 (References 2.5-234 and 2.5-241). The updated seismicity catalog in Section 2.5.2.1 designates the Mineral earthquake as **M** 5.8. The Mineral earthquake resulted from reverse faulting at a relatively shallow depth, approximately 4.7 mi (7.5 km), in central Virginia

(Figure 2.5.1-201) (References 2.5-232, 2.5-235, and 2.5-237). More recent analyses indicate that the main shock hypocenter originated at 6.0 ± 3.1 km depth (Reference 2.5-268). Additional information on the Mineral earthquake is presented in Sections 2.5.2.1.3 and 2.5.2.2.5.1. Seismicity in this region is attributed to the CVSZ, as described above.

In order to best represent the approximate rupture plane or fault that produced the Mineral earthquake, the aftershock information provided on the Virginia Tech Seismological Observatory (VTSO) website (Reference 2.5-242), and described in Section 2.5.1.1.7, was used to develop a representation of the possible rupture plane and its up-dip projection to the surface (Figure 2.5.1-203). These seismologic data, analyses, and the results of a geological reconnaissance indicate that there is no evidence of surface rupture or deformation of the ground surface. See Sections 2.5.1.1.7 and 2.5.2.3 for further descriptions of this topic. A few liquefaction features were generated by the Mineral earthquake and are described by researchers who investigated the epicentral area immediately following the earthquake (References 2.5-233, 2.5-243, 2.5-398, and 2.5-402).

In the days immediately following the August 23, 2011 Mineral, Virginia earthquake, an Earthquake Engineering Research Institute (EERI) Geotechnical Extreme Events Reconnaissance (GEER) team of engineers and geologists performed regional ground reconnaissance and identified two sites along the South Anna River where liquefaction occurred (EERI 2011) (Reference 2.5-402) (Figure 2.5.1-225). Two liquefaction features described as “sand boils” are identified by the GEER reconnaissance team at the Yancey-3 site (Figure 2.5.1-225). The Yancey-3 site is located within the incised river channel of the South Anna River near Yanceyville, Virginia, approximately 25 meters downstream of the old mill dam near the intersection of Yanceyville Road and Vigor Road. These sand boils are small and located along the southeast margin of the South Anna River (Green et al. 2014) (Reference 2.5-398). At the time of reconnaissance, the water level in the river was relatively low but the groundwater saturated zone likely was only a few centimeters below the ground surface (Green et al. 2014). The material ejected from these two sand boils is described as well-graded sand with silt and gravel (SW-SM) (Green et al. 2014).

One liquefaction feature described as a small “sand boil” is identified by the GEER team at the BOR-2 site (Figure 2.5.1-225). The BOR-2 site is

located within a tributary drainage channel of the South Anna River, approximately 3 km northwest of the Yancey-3 site and near the Bend of River housing subdivision. The material ejected from this sand boil is described as silt (ML) (Green et al. 2014).

Investigations at both the Yancey-3 and BOR-2 sites indicate that although the sand boils likely resulted from liquefaction, the material properties, stratigraphy, and source zone of liquefaction were less than ideal (EERI 2011). Further, the magnitude and period of the 2011 Mineral earthquake was lower than would be expected to generate wide-spread liquefaction given ideal conditions (low density, clean and saturated sand capped by a local confining layer).

Obermeier and McNulty (1998) (SSAR Reference 71) identify two paleoliquefaction sites in the CVSZ (Figure 2.5.1-225). At the JAR-1 site on the James River, Obermeier and McNulty (1998) describe abundant river bank exposures with “only a few small [clastic] dikes of very restricted geographic extent.” Radiocarbon data and the lack of any weathering in the host sediment at this site suggest that the clastic dikes have an age of less than a few hundred years (Obermeier and McNulty 1998). They describe the Cedar Branch-1 site on the Rivanna River as including “a few small severely weathered [clastic] dikes (?) penetrated into host deposits that could be as old as early Holocene, on the basis of severity of weathering.” A third site of possible early- to mid-Holocene liquefaction may also be present at the SAR-3 site on the South Anna River (Dominion 2004) (Reference 2.5-404).

Based on the scarcity and limited geographic extent of identified paleoliquefaction features in the Central Virginia region, Obermeier and McNulty (1998) conclude that earthquakes of **M** 7 or larger are not likely to have occurred in their study region in the last 2,000-3,000 years, or, in the eastern portion of their study region, in the last 5,000 years. Furthermore, they conclude, “Smaller earthquakes could have struck but not be recorded in the paleoseismic record of our study area, but even if **M** 6-7 earthquakes had been relatively abundant, then many more liquefaction effects would have been expected.”

The isolated locations of small paleoliquefaction features in the CVSZ are consistent with the isolated and relatively small 2011 liquefaction features, suggesting that the paleoliquefaction features may have been produced by local, moderate-magnitude earthquakes similar to the 2011 Mineral earthquake. Thus, the seismic source characterization for the

region surrounding the North Anna site is enveloped by the CEUS-SSC model, which includes a large Mmax distribution for the host source zone (ECC-AM) and recurrence parameters (a- and b-values) derived from the historical seismicity.

2. Giles County Seismic Zone

The fourth paragraph of Item 2 under Item d of this SSAR section is replaced as follows.

NAPS ESP VAR 2.0-4

The largest known earthquake to occur in this region is the 1897 **M** 5.9 Giles County event (Section 2.5.2.1.3). Bollinger (SSAR Reference 79) estimated an M_{max} of m_b 6.3 for the Giles County seismic source using three different methods. Chapman and Krimgold (SSAR Reference 57) used an M_{max} of m_b 7.25 for the Giles County zone and most other sources in their seismic hazard analysis of Virginia. These estimates of maximum magnitude earthquakes are incorporated in the CEUS SSC model as summarized in Sections 2.5.2.2 and 2.5.2.3. This zone is currently recognized as comprising a portion of the PEZ (Reference 2.5-223).

3. Selected Seismogenic and Capable Tectonic Sources Beyond the Site Region

The fifth paragraph under Eastern Tennessee Seismic Zone of Item 3 under Item d of this SSAR section is replaced as follows.

NAPS ESP VAR 2.0-4

Using three different methods specific to the Eastern Tennessee seismic source, Bollinger (SSAR Reference 79) estimated an M_{max} of m_b 6.45. Chapman and Krimgold (SSAR Reference 57) used an M_{max} of m_b 7.25 for the Eastern Tennessee zone and for most other sources in their seismic hazard analysis of Virginia. Both of these more recent estimates of M_{max} are similar to the range of M_{max} values used in the 1986 EPRI studies. These estimates of maximum magnitude earthquakes are incorporated in the CEUS SSC model as summarized in Sections 2.5.2.2.5.2 and 2.5.2.3.

	The last sentence of the third paragraph under **Charleston Seismic Zone** of Item 3 under Item d of this SSAR section is replaced as follows.
NAPS ESP VAR 2.0-4	The Charleston Zone as defined by the CEUS SSC Project is characterized by evidence of RLMEs (Reference 2.5-223). The Charleston RLME is described in Sections 2.5.2.2.4.1 and 2.5.2.3.
	A sentence is added to the end of the fourth paragraph under **Charleston Seismic Zone** of Item 3 under Item d of this SSAR section as follows.
NAPS ESP VAR 2.0-4	These estimates of maximum magnitude earthquakes and recurrence rates are incorporated in the CEUS SSC model as summarized in Section 2.5.2.2.4.1. The Charleston RLME is discussed in Section 2.5.2.3.
NAPS ESP VAR 2.0-4	The last paragraph under **Charleston Seismic Zone** of Item 3 under Item d of this SSAR section is deleted.
	The first paragraph under **New Madrid Seismic Zone** of Item 3 under Item d of this SSAR section is replaced as follows.
NAPS ESP VAR 2.0-4	The New Madrid Seismic Zone extends from southeastern Missouri to southwestern Tennessee and is over 620 miles west of the Unit 3 site. The New Madrid Seismic Zone is one of four RLME sources that comprise the Reelfoot Rift Zone as defined by the CEUS SSC (Figure 2.5.1-202) (Reference 2.5-223) and is defined by post-Eocene to Quaternary faulting and historical seismicity.
	The last sentence of the sixth paragraph under **New Madrid Seismic Zone** of Item 3 under Item d of this SSAR section is replaced as follows.
NAPS ESP VAR 2.0-4	These estimates of maximum magnitude earthquakes and recurrence rates are incorporated in the CEUS SSC model as summarized in Section 2.5.2.2.4.2. The New Madrid Fault system RLME is discussed in Section 2.5.2.3.
NAPS ESP VAR 2.0-4	The last paragraph under **New Madrid Seismic Zone** of Item 3 under Item d of this SSAR section is deleted.

NAPS ESP VAR 2.0-4

2.5.1.1.6 Geologic Bases for Defining Relevant Source Zones

As stated above, the Unit 3 site is located within the ECC-AM seismotectonic source zone (Figure 2.5.1-202) (Reference 2.5-223). This zone is defined to include the region characterized by the presence of rifted and extended continental crust that developed as a result of Mesozoic rifting that resulted in the formation of the Atlantic Ocean. A tectonic feature of the Mesozoic extended crust within the ECC-AM is an older east-dipping basal detachment fault (decollement) that separates overthrusted Appalachian terranes from underlying Precambrian rocks of the North American craton (Section 2.5.1.1.4.c.1, SSAR Figures 2.5-2 and 2.5-8, and Reference 2.5-223). The tectonic evolution of the site region is summarized in SSAR Section 2.5.1.1.2 and Section 2.5.1.1.4.a. Seismicity within the ECC-AM is discussed in Sections 2.5.2.2.3.1 and 2.5.2.3. Johnson et al. (SSAR Reference 195) present a global study of earthquakes in stable continental regions (SCRs). This study and the update in the CEUS SSC (Reference 2.5-223) document the assessments that Mesozoic and younger extended crust has produced all **M** ≥ 7 stable craton earthquakes worldwide.

The PEZ is the seismotectonic zone located immediately west of the ECC-AM (Figure 2.5.1-202) (Reference 2.5-223). The definition of this zone is also based on the studies documented in SSAR Reference 195 and updates documented in Reference 2.5-223 that late Precambrian to early Paleozoic rifting (Iapetan crustal extension) formed zones of crustal weakness that exhibit a higher rate of seismic activity. The Iapetan rifted margin defined in SSAR Reference 49 includes that part of the continental crust that includes known or inferred normal faults that formed parallel to the passive margin of Laurentia during the late Proterozoic to early Paleozoic opening of the Iapetus Ocean (Reference 2.5-223). These faults occur in the older crust beneath the Appalachian decollement and appear to be the structures along which earthquakes in the Giles County zone (Section 2.5.1.1.4.d.2) and East Tennessee zone (Section 2.5.1.1.4.d.3) occur. Figure 2.5.1-202 shows the PEZ Wide (PEZ-W). This is an alternative geometry of the PEZ that is extended to the west to incorporate additional Iapetan-rifted crust. The western boundary of the PEZ-W follows the Rome trough in Kentucky and West Virginia, following the Kentucky River fault system (Reference 2.5-223). Seismicity within the PEZ is discussed in Sections 2.5.2.2.3.3 and 2.5.2.3.

The AHEX seismotectonic zone represents the region of highly extended crust that is the transition between the extended, thick continental crust that underlies the ECC-AM and the thinner mafic oceanic crust of the Atlantic Ocean basin (Figure 2.5.1-202) (Reference 2.5-223). This zone is located entirely offshore and approximates the continental shelf from Nova Scotia to Georgia. The eastward thinning wedge of highly extended transitional crust forming the AHEX is significantly thinner than the extended continental crust of the ECC-AM. This zone is characterized by a greater amount of rifting that resulted in both a thinner crust and the introduction of basalts and mafic intrusions. The transition crust of the AHEX appears to correspond with the East Coast magnetic anomaly and is mainly defined on the basis of these geophysical data (Reference 2.5-223). Seismicity within the AHEX is discussed in Sections 2.5.2.2.3.2 and 2.5.2.3.

NAPS ESP VAR 2.0-4

2.5.1.1.7 Information on the Mineral Earthquake

a. **Seismicity**

The August 23, 2011 **M** 5.8 Mineral earthquake resulted from reverse faulting at a relatively shallow depth, approximately 4.7 mi (7.5 km), in central Virginia (Figure 2.5.1-201) (References 2.5-232, 2.5-235, and 2.5-237). More recent analyses indicate that the main shock hypocenter originated at 6.0 ± 3.1 km depth (Reference 2.5-268) or 7 ± 2 km (Reference 2.5-392). Seismicity in this region is attributed to the CVSZ, a previously recognized zone of seismicity that has produced numerous historical small and moderate earthquakes (see Section 2.5.1.1.4.d.1). The largest earthquake prior to the Mineral earthquake occurred in 1875 and had an estimated magnitude of about **M** 4.8 based on felt reports and reported damage (Reference 2.5-244). The most recent damaging earthquake prior to the Mineral earthquake was a magnitude 4.5 on December 9, 2003 (Reference 2.5-244). Both of these prior earthquakes were in Goochland County, VA, near the James River and south of the Mineral earthquake epicenter.

McNamara et al. (2014) (Reference 2.5-392) compiled a catalog of 395 aftershocks associated with the Mineral earthquake, including relocated aftershocks from 36 stations deployed in the first few days following the mainshock. The locations and focal mechanisms from the Mineral earthquake main event and numerous aftershocks indicate a rupture plane that strikes approximately N36°E and dips approximately 49.5°ESE, slightly oblique to the regional structural grain

(Reference 2.5-392). The focal mechanism solutions presented by McNamara et al. (2014) for the Mineral earthquake main event and aftershocks principally are reverse-slip.

The map view pattern of aftershocks in McNamara et al.'s (2014) catalog reveals three clusters of seismicity surrounded by a broader region of more diffuse seismicity (Figure 2.5.1-208). The westernmost cluster of aftershocks encompasses the **M** 5.8 mainshock, is the largest and densest of the clusters, and defines an approximately 10-km-long, northeast-trending zone up to about 6 km wide (Figure 2.5.1-209). Hypocenter depths in this main cluster decrease systematically along a northwest gradient from about 8 km to 2 km depth. Several studies, including Horton et al. (2012b) (Reference 2.5-232), Shao et al. (2012) (Reference 2.5-240), Chapman (2012) (Reference 2.5-235), Chapman (2013) (Reference 2.5-397), and McNamara et al. (2014), describe the main aftershock cluster as tabular or planar and approximate the main cluster with best-fit planes. These best-fit planes are intended to represent approximations of the location and geometry of the Mineral earthquake source, which Horton et al. (2012a) (Reference 2.5-223) have named the Quail fault. In general, these studies indicate that the rupture plane strikes about N30°E and dips about 45° to 55°SE. McNamara et al. (2014) used a bootstrap method to estimate the uncertainty in the geometry of the rupture plane from relocated aftershock data, calculating a strike of N36°E ±12° and dip of 49.5°SE ±6°. Figure 2.5.1-209, which is modified from McNamara et al. (2014), presents section lines, a cross-section oriented approximately orthogonal to the strike of the rupture plane defined by Mineral earthquake aftershocks, and a cross-section along strike of the rupture plane. Figure 2.5.1-209 depicts the approximate locations of the up-dip and vertical surface projections of the rupture plane defined by McNamara et al. (2014). In an earlier interpretation of aftershock data, Horton et al. (2012a) described the rupture surface as slightly concave-up, an interpretation of the rupture geometry that is not described by others and remains unique to that publication.

The easternmost subsidiary cluster of seismicity covers the second largest area, lies about 10 km east of the main cluster, and defines an approximately 7-km-long, northeast-trending zone up to about 2 km wide (Figure 2.5.1-208). Aftershock depths in this cluster are generally less than 4 km, with local magnitudes of 2.6 or less. The third and smallest

cluster, located between the two described above, defines an approximately 1-km-radius, irregular zone of aftershocks with local magnitudes of 2.5 or less, and depths generally less than 3 km.

No studies have formally defined rupture planes or attempted to characterize potential sources from aftershocks in the subsidiary clusters described above. Furthermore, McNamara et al. (2014) developed only one focal mechanism for an aftershock lying outside of the main cluster, and its orientation is significantly different than focal mechanisms of main cluster events. McNamara et al. (2014) indicate that aftershocks in these shallow subsidiary clusters occurred relatively late and suggest that they were triggered by stress transfer due to earlier activity in the main cluster. These clusters, therefore, likely represent minor triggered slip on multiple, minor shears of limited extent in a zone of highly deformed bedrock.

An additional cluster of aftershocks was identified by Horton et al. (2012a and 2012b). This cluster is northwest of the main cluster, dips to the northwest, and terminates up-dip at its intersection with the Mineral earthquake rupture plane. No other studies or maps make note of this cluster, the interpretation of which seems to be limited to Horton et al. (2012a and 2012b). Furthermore, no features matching that description are readily apparent in the recent catalog and aftershock cross-section constructed by McNamara et al. (2014). It is possible that this additional cluster and associated structure by Horton et al. (2012a and 2012b) may have been a product of their interpretation of an early aftershock catalog.

b. Geologic Reconnaissance

A geologic field reconnaissance was conducted between April 19-21, 2012 to evaluate and document whether the August 23, 2011 **M** 5.8 Mineral earthquake produced coseismic surface rupture or other visible forms of surface deformation. To aid in the geomorphic and geologic assessment of the Mineral earthquake study area, Light Detection and Ranging (lidar) data were acquired to produce high-resolution topographic images in the epicentral area (Figure 2.5.1-207). The lidar data were processed to produce a bare earth model, which eliminates above ground points such as the tree canopy. The lidar package included:

- Digital Elevation Model (DEM)
- Hillshade Map

- Slope Map
- Contour Map (1 ft contour interval), and
- Orthophotography

In order to best represent the approximate rupture plane or fault that produced the Mineral earthquake, the aftershock information from various authors and as provided on the VTSO website (Reference 2.5-242) were used to develop a representation of the possible rupture plane and its up-dip projection to the surface. These findings are summarized as follows:

- "This cluster [of aftershock hypocenters] spans a lateral distance of ~10 km and is centered beneath Yanceyville on the South Anna River. The best fit plane to this cluster, the Quail fault (QF) strikes N30°E and dips 46°SE" (Reference 2.5-232).
- "The early aftershocks define a plane striking N29°E and dipping 51 degrees to the southeast" (Reference 2.5-235).
- "Given the regional trend of the geology and aftershock distribution, we prefer a fault plane that has a strike of 28 degrees and a dip of 55 degrees based on the University of Saint Louis regional CMT solution" (Reference 2.5-240).
- "The inferred plane dips down 46 degrees to the east-southeast" (Reference 2.5-241).

The up-dip surface projection, as shown on Figure 2.5.1-203, approximates where the fault may intersect the ground surface. Constraining the approximate location of the Mineral earthquake rupture plane allows for comparisons with the surface geology and geomorphology to assess the potential for surface deformation from the 2011 Mineral event or any past surface ruptures preserved in the landscape. Figure 2.5.1-203 was created in the following manner:

- Hypocenters from Reference 2.5-242 were plotted (color-coded by depth) along with the surface-projected aftershocks. The aftershocks were projected up-dip to the surface along a plane oriented N29°E and dipping 51°SE. The surface-projected aftershocks represent a best estimate of where the fault rupture would intersect the ground surface.

- A best-fit line was drawn through the surface-projected aftershocks (shown as a dark red dashed line on Figure 2.5.1-203). The orientation and length of this up-dip surface projection are N30°E and 6.2 mi (10 km), respectively.
- An estimate of the vertical surface projection of the rupture plane was developed using information from Horton et al. and is shown as a red dashed rectangle on Figure 2.5.1-203. This plane is approximately 0.62 mi (1 km) southeast of the up-dip surface projection, consistent with an approximately 45° dip and an estimated 0.62 to 4.7 mi (1 to 7.5 km) depth (Reference 2.5-232). The rectangle represents the approximate vertical projection of a rupture plane with a dip of 46 to 51° from an upper depth of about 0.62 mi (1 km) and a lower depth of about 4.7 mi (7.5 km).

This interpretation shown on Figure 2.5.1-203 depicts an area where any surface rupture would likely be located. The subtle differences in strike and dip estimated by the seismologists cited above are considered as inherent uncertainty in the aftershock location calculations.

The field reconnaissance focused primarily on the areas of the up-dip surface projection and the vertical surface projection of the rupture plane (Figure 2.5.1-204). To account for uncertainty, the reconnaissance covered a broad area surrounding these projections. Several other areas that were also evaluated included the epicentral area along Shannon Hill Road, reported damage in the towns of Louisa and Mineral, road crossings of mapped faults, and the area immediately west of the North Anna site (Figure 2.5.1-204).

The area of field reconnaissance was evaluated for evidence of recent surface faulting from the 2011 Mineral earthquake, as well as evidence of repeated surface faulting. Subtle geomorphic evidence in the landscape may indicate where repeated surface or blind faulting may have occurred. Evidence for potential surface faulting or deformation varies based on the perspective or scale of observations as well as the age and recurrence of potential past events. Prior to and following completion of the field reconnaissance, information in the lidar data collected for this study and derivative products were evaluated for evidence of regional fault-related geomorphic features, including geomorphic lineaments caused by active faulting, stream gradient changes or offsets, and contrasting large topographic features. Some of these evaluations are further discussed below.

The geologic field reconnaissance evaluated local geomorphic and anthropogenic features for more direct evidence of surface rupture associated with the Mineral earthquake. Based on the lack of field evidence immediately following the Mineral earthquake, the size of the postulated rupture plane, and the moderate magnitude of the earthquake, significant evidence for surface rupture was not anticipated and therefore efforts were focused on detecting other possible minor surface effects. Additionally, given the lack of numerous outcrops and exposures in the area, the field reconnaissance primarily focused on searching for evidence of recent rupture and deformation of roads and roadway corridors, and confirming previously mapped geologic units as well as obtaining familiarity with the regional geology and geomorphology to better aid in interpretation of the lidar data.

Figure 2.5.1-204 shows the routes and waypoints of the field reconnaissance and the numerous roads that cross the projected surface trace of the rupture surface at oblique to near orthogonal angles. The pavement on these roads was in good condition and showed minimal distress cracking from age or settlement, making them excellent strain markers. No deformation in paved road surfaces was detected during the survey.

Based on available data and published information, there is no evidence to support a Mineral earthquake rupture plane that is characterized by a significantly different geometry or location than shown on Figure 2.5.1-203. Similarly, subsidiary aftershock clusters do not appear to be structurally linked with the Mineral earthquake aftershock plane. Therefore, deformation associated with the Mineral earthquake would be most likely expected in the vicinity of the up-dip projection of the best-fit plane, or above the vertical projection of the best-fit plane (i.e., hanging wall). Therefore, both of these areas received the greatest focus for geologic field reconnaissance. During transects of the reconnaissance area, Dominion's geologists traversed roads several kilometers north and south of the up-dip projection of the rupture plane to account for uncertainty in dip and for various up-dip fault geometries (Figure 2.5.1-204). Specifically, the field reconnaissance team looked for field evidence of surface deformation or faulting that included:

- Ground fissures or compressional ground buckling;
- Minor fault scarps;

- Fault controlled drainages;
- Cracked or offset pavement along roads;
- Springs or artesian conditions; and
- Changes in vegetation growth.

Dominion's reconnaissance team did not find any evidence of tectonic surface deformation related to the Mineral earthquake. No previous studies have found evidence suggestive of, or that demonstrates, surface rupture related to the Mineral earthquake.

c. Geologic Aspects of the Mineral Earthquake Epicentral Region

New interpretations of the geology in the Mineral earthquake epicentral region have emerged following the earthquake and further research will likely continue for several years. Geologic maps of this area, which is characterized by gentle topography and limited bedrock exposures, include considerable interpretation and uncertainty. Hughes and Hibbard (2012) (Reference 2.5-246) and Burton et al. (2014) (Reference 2.5-396) have reinterpreted the locations of the Chopawamsic and Long Branch faults, and have defined additional structures.

The Chopawamsic fault was the nearest mapped fault to the approximate up-dip projection of the Mineral earthquake rupture plane based on maps of Marr (2002) (SSAR Reference 105) and Mixon et al. (2000) (SSAR Reference 44) (Figure 2.5.1-210A). Subsequent mapping by Hughes and Hibbard (2012) (Figure 2.5.1-210B) and Burton et al. (2014) (Figure 2.5.1-210C) suggests that the Chopawamsic fault lies several kilometers northwest of the earlier depictions. The mapping by Hughes and Hibbard (2012) removes the prominent fold in the fault and adjacent units. Burton et al.'s (2014) mapping shows that the Chopawamsic fault separates the Chopawamsic Formation from older rocks to the northwest (Figure 2.5.1-210C). Burton et al.'s (2014) mapping also places a fault contact (Harris Creek fault) between the Chopawamsic Formation and the Ellisville pluton. The more northwesterly location of the Chopawamsic fault reduces the likelihood that the fault was the source of the Mineral earthquake and suggests that the rupture plane (i.e., Quail fault of Reference 2.5-232) lies structurally above (and east of) the Chopawamsic fault. The contact between the Chopawamsic Formation and the Ellisville pluton is mapped as the Harris Creek fault by Burton et al. (2014) (Figures 2.5.1-211A and 2.5.1-211B).

The mapped location of the Long Branch fault varies by source. Mapping by Marr (2002) (Figure 2.5.1-210A) depicted the Long Branch fault extending southwest through the epicentral area of the Mineral earthquake. A map image from a conference presentation by Hughes and Hibbard (2012) depicted at a very small scale a similar southwestern extension based on exposure of L-tectonite along the South Anna River. Mapping by Dicken et al. (2005) terminates the Long Branch fault to the northeast, outside of the epicentral area, but with a strike oriented toward the epicentral area. More recent mapping by Burton et al. (2014) also relies on the exposure of L-tectonite as evidence to extend and constrain the location of the Long Branch fault to the southwest (Figures 2.5.1-210C and 2.5.1-211A). Their depiction of the Long Branch fault lies about 1 km northwest of the mapped trace of Marr (2002), which also extends southwest into the epicentral area. Burton et al. (2014) depict the Long Branch fault striking about N35°E and separating 40° to 50° dipping subunits of the Chopawamsic Formation, suggesting that the dip of the fault is likely about the same.

Abstracts published shortly following the Mineral earthquake considered the Long Branch fault a likely source of the Mineral earthquake, based primarily on its proximity to the epicentral area. For example, Hughes and Hibbard (2012) describe the Long Branch fault as an imbricate fault within the Chopawamsic Formation and suggest that it represents the most likely of previously mapped faults to be the source of the Mineral earthquake. Harrison et al. (2011) (Reference 2.5-401) interpret a linear magnetic anomaly that is oriented similar to the Long Branch fault as a possible southwestern extension of the Long Branch fault and further suggest that recent seismicity possibly occurred on the fault near its subsurface intersection with Mesozoic structures.

The relationship of the surface trace of the Long Branch fault with the aftershocks, however, suggests it is not the source of the Mineral earthquake. The surface trace of the Long Branch fault as mapped by Burton et al. (2014) overlies aftershocks of the main cluster that lie about 4 km deep. Similar relationships are observed in mapped fault traces by Marr (2002) and Hughes and Hibbard (2012). Projection of the trace by Dicken et al. (2005) to the southwest also exhibits a similar relationship with the aftershocks. Mineral earthquake aftershocks define a dipping plane (e.g., Horton et al. 2012a; Chapman 2013; McNamara et al. 2014) that projects up-dip to the ground surface 3 to 4 km north of the mapped

surface traces of the Long Branch fault (Figure 2.5.1-209). This structural relationship indicates that the Long Branch fault is structurally higher than, and is approximately parallel with, the rupture plane of the Mineral earthquake. Therefore, as it is presently mapped, the Long Branch fault likely does not represent the source of the Mineral earthquake.

Thus, it appears the rupture plane lies structurally above (and east of) the Chopawamsic fault, and structurally below (and west of) the Long Branch fault, and the source of the Mineral earthquake seems to be located between these two southeast-dipping faults in the subsurface. Green et al. (2014, p. 7) (Reference 2.5-398) propose an alternative explanation for the source of the Mineral earthquake, noting "the planar but diffuse group of aftershock hypocenters defining the Quail fault at depth may reflect a zone of rupture along a composite of rock structures, including litho-rheological contrasts, Paleozoic foliations, and Mesozoic to Cenozoic joint sets, all favorably oriented to slip by regional- and local-stress geometry."

Two northerly-striking Jurassic dikes are mapped by Burton et al. (2014) across the Chopawamsic, Harris Creek, other unnamed faults, and the up-dip projection of the Mineral earthquake rupture plane (Figures 2.5.1-210C and 2.5.1-211A). The dikes are described as fine-grained diabase up to 10 m in width. The lack of any discernible offset of these dikes in map view significantly limits the amount of post-Jurassic displacement on any of these structures. Burton et al. (2014) (Reference 2.5-396, p. 107), however, state that one dike shows a "slight offset across the eastern contact of the Ellisville neck, accompanied by float of quartz breccia," suggesting post-intrusive brittle reactivation of the contact between the Ellisville pluton and Chopawamsic Formation.

d. Geomorphic Aspects of the Mineral Earthquake Epicentral Area

This section describes geomorphic observations of the Mineral earthquake epicentral area by Dominion geologists and from the published literature. To evaluate the presence or absence of geomorphic evidence for tectonic deformation in the epicentral area of the Mineral earthquake, Dominion geologists used lidar and other topographic data to make basic geomorphic observations, develop longitudinal stream profiles, and develop topographic ridge profiles. These geomorphic evaluations were performed primarily as desktop studies. Additionally, this section describes recent abstracts by Berti et al. (2012)

(Reference 2.5-394) and Harrison (2012) (Reference 2.5-400), which describe localized geomorphic features that they suggest may represent Quaternary tectonic deformation in the Mineral earthquake epicentral area.

1. Basic Geomorphic Observations

Dominion's review of lidar data from the vicinity of the Mineral earthquake indicates that many topographic lineations appear to be lithologically controlled and are associated with changes in rock type and the differences in erodibility between rock types. Figures 2.5.1-211A, 2.5.1-211B, 2.5.1-212A, and 2.5.1-213 illustrate an abundance of topographic lineaments along bedrock contacts, dikes, and internal erosion contrasts within geologic units. Alignments of short discontinuous features in the landscape are abundant throughout the area of lidar coverage (using enhanced slope maps), are commonly parallel to structural grain, and most likely represent erosional susceptibility contrasts between differences in lithology. These observations indicate the strong control of bedrock structure on the landscape.

A topographic lineament is associated with the Harris Creek fault, which lies within the area of uncertainty defining the up-dip projection of the 2011 Mineral earthquake aftershock plane. The Harris Creek fault of Burton et al. (2014) (Figure 2.5.1-210C) is expressed as a subtle topographic lineament (black arrows on Figure 2.5.1-211A) and as differences in relief (dotted outline of pluton on Figure 2.5.1-212A). The topographic lineament is composed of two elements: 1) a general northwest-facing slope; and 2) a break in that slope with steeper slopes (dark shading) consistently along the southern margin. The terms "escarpment" and "topographic lineament" are used interchangeably to refer to this feature that can be observed on Figure 2.5.1-211B.

As mapped by Burton et al. (2014) (Reference 2.5-396), the Harris Creek fault is a southeast-dipping reverse fault with a strike of about N50°E, and a minimum length of approximately 14.5 km. The fault extends from the northern boundary of the Burton et al. (2014) map where it lies within mylonitic rocks of the Chopawamsic Formation to the southwest where it separates the Ellisville pluton tail from the Chopawamsic Formation (Figures 2.5.1-210C and 2.5.1-216).

The expression of this topographic lineament, however, does not extend to the northeast portion of Figures 2.5.1-211A and 2.5.1-211B where the

fault bifurcates and no longer juxtaposes these two units. These observations support a lithologic, as opposed to tectonic, explanation for the geomorphic expression along the margins of the pluton. The Harris Creek fault lies in close proximity to, or coincident with, the northwest-facing geomorphic escarpment along approximately 10 km of its mapped extent. The topographic lineament does not extend southwest and northeast beyond the South Anna River drainage, as there is no geomorphic expression in the drainage divides.

The observations define a nearly continuous northwest-facing escarpment and break in slope approximately coincident with the Harris Creek fault only where it crosses the South Anna River valley. The most likely explanation is that this topographic lineament is an erosional feature controlled by juxtaposed lithologies and not the result of neotectonic activity associated with the Harris Creek fault. This interpretation is supported by the following rationale:

- The region exhibits an abundance of subtle topographic lineaments that correlate to mapped lithologic contacts (unfaulted). Differences in rock resistance is observed at both map scale between formations and at outcrop scale between alternating lithologies within a particular formation (i.e., highly weathered schist vs. fresh, quartz-rich rock).
- For almost its entire length, the northwest-facing escarpment separates more resistant rocks (Chopawamsic Formation) on the uphill side and less resistant rocks (granodiorite) on the downhill side.
- Where the main fault lies entirely within the Chopawamsic Formation, it is not expressed geomorphically.
- The better pronounced portions of the escarpment are located near the bottom of the South Anna River valley, where rates of erosion are presumably greatest. This also appears to be the “neck” or “tail” of the Ellisville pluton where foliation may have made the granodiorite less resistant to erosion.
- The geomorphic expression appears to die out both northeast and southwest at broad, gently sloping drainage divides, where rates of erosion are presumably the lowest.

While these observations strongly support a lithologic explanation for the geomorphic features observed along the Harris Creek fault, they cannot completely rule out minor neotectonic slip on the Harris Creek fault. However, given the lack of observable surface deformation during the

2011 **M** 5.8 Mineral earthquake, it is unlikely that repeated events of this magnitude would be recorded in the landscape. That is, larger magnitude events would likely be necessary to produce surface ruptures and a topographic expression in the landscape. Such events would require much larger fault dimensions that extend well beyond the mapped trace of the Harris Creek fault and the topographic lineament.

High relief values within the lidar study area appear to be highly influenced by two factors: 1) higher erosion rates concentrated along the South Anna River valley; and 2) the underlying lithology of the Ellisville granodiorite pluton tail. Figure 2.5.1-212A presents a hillshaded relief (i.e., elevation difference) map. Colors in this map correspond to the range of local elevation within 0.5 km of any given point. Figure 2.5.1-212B presents a hillshaded elevation map that utilizes a linear color ramp, and also uses the same symbolization scheme as the relief map (Figure 2.5.1-212A) for a more direct comparison.

As shown on Figure 2.5.1-212A, a relief lineament is located within the brackets outlining the area of uncertainty for the up-dip projection of the 2011 Mineral earthquake rupture plane (termed the Quail fault by Horton et al (2012) (Reference 2.5-232)). This relief lineament, which separates higher relief on southeast and lower relief on northwest, could be interpreted to represent a more concentrated area of incision responding to long-term uplift in the hanging wall of a southeast-side-up reverse fault. However, a more plausible interpretation is that the relief lineament represents differences in the weathering and denudation of adjacent rock types for several reasons. First, the opposite margin of the pluton tail exhibits a similar relief lineament with lower relief in the granodiorite rock and higher relief in the Chopawamsic Formation. This produces a relatively low relief region corresponding to the neck or tail of the pluton (Figure 2.5.1-212A). High relief is concentrated on both sides of the pluton in the Chopawamsic Formation and not only in the hanging wall of the 2011 Mineral earthquake rupture. Second, these relief lineaments are nearly coincident with both contacts of the Ellisville granodiorite tail, which strike a little more easterly than the rupture plane or the Harris Creek and Roundabout faults (Figure 2.5.1-212A). Third, the highest relief values are concentrated near the intersection of the northwest margin of the pluton tail and the South Anna River, which suggests both the rock type and incision along the river influences the map pattern of relief.

The most continuous areas of low relief can be found along prominent drainage divides and areas of higher elevation, which represent areas farthest removed from the increased erosion rates associated with trunk streams (Figures 2.5.1-212A and 2.5.1-212B).

The South Anna River approximately bisects the rupture plane rectangle (Figures 2.5.1-212A). Therefore, the relief values are not only decreasing with distance from the rupture plane rectangle, they are also diminishing away from the axis of the South Anna River valley, an expected result of the higher erosion rates and long term incision associated with a river valley. The observations of the relief map (Figures 2.5.1-212A) support the interpretation of a landscape that is highly influenced by erosion rates that increase toward major drainages, and the interplay of erosion rates with rocks of variable lithology.

2. Stream and Topographic Ridge Profiles

As part of Dominion's geologic field reconnaissance program to evaluate possible surface deformation associated with the Mineral earthquake, analyses of stream profiles in the epicentral region were performed. Longitudinal profiles were constructed for five tributary streams that drain into the South Anna River in the epicentral area and topographic profiles were constructed for the crests of two interfluves (ridgelines) located in the epicentral area (Figures 2.5.1-214 through 2.5.1-216). For portions of profiles within Area A of project lidar coverage, elevations were extracted from this 2 foot horizontal resolution lidar dataset. For portions of profiles outside of lidar Area A, elevations were extracted from the 10 m horizontal resolution National Elevation Dataset (NED). The 10 m NED was included to extend profiles into headwaters, but identification of anomalies focused on lidar portions of the profiles, which traversed the surface projection of 2011 rupture plane. Except where noted, the profiles are vertically exaggerated 25 times. This exaggeration is needed to illustrate the very subtle forms and gradient changes in this very low-relief topography. A summary of the two prominent and three other very subtle gradient changes on stream profiles is included in Table 2.5.1-201.

In general, stream profiles are well graded and do not exhibit any unusual geomorphic form (Figures 2.5.1-217 through 2.5.1-224). The set of profiles were initially evaluated against geologic mapping compiled from the 1:100,000 scale geologic maps of Marr (2002) (SSAR Reference 105) and Mixon et al. (2000) (SSAR Reference 44), the 1:500,000 scale geologic map of Dicken et al. (2005)

(Reference 2.5-245), and a portion of the Ferncliff 7.5 minute quadrangle presented by Hughes and Hibbard (2012) (Reference 2.5-246). These maps were used initially because they covered the full extent of the profiles and represented the most recent mapping at that time. The profiles were created prior to the publication of the Burton et al. (2014) geologic mapping. The more detailed Burton et al. (2014) geologic map (Reference 2.5-396) post-dates the 2011 Mineral earthquake, represents the most detailed mapping of the epicentral area, and also includes a slightly different location of the Chopawamsic fault from previous mapping (with the exception of Hughes and Hibbard, 2012).

The profiles presented in Figures 2.5.1-217 through 2.5.1-224 demonstrate that streams crossing the epicentral area are very well graded. They also demonstrate that there are no significant anomalies associated with the up-dip projection of the 2011 rupture plane or any of the faults mapped by Burton et al. (2014), including the Harris Creek fault.

Profiles included are Beaver Creek (Figure 2.5.1-217), Contrary Creek (Figure 2.5.1-218), Harris Creek (Figure 2.5.1-219), Mt. Airy Road Ridge (Figure 2.5.1-220), Northeast Creek (Figure 2.5.1-221), Roundabout Creek (Figure 2.5.1-222), South Anna River (Figure 2.5.1-223), and Yanceyville Road Ridge (Figure 2.5.1-224). The locations of these profiles are shown in Figure 2.5.1-216, which incorporates a geologic base map from Burton et al. (2014).

Two anomalously steep gradients are observed in the stream profiles. One is located on Harris Creek and the other on Beaver Creek (Figure 2.5.1-217). Neither of these stream anomalies appear to correlate with the up-dip projection of the rupture plane, the Harris Creek fault, Roundabout Farm fault, or other faults. These two anomalously steep gradients, however, are located on or near the contact between Chopawamsic Formation and the Ellisville granodiorite (Figure 2.5.1-216). Only these two prominent anomalies are labeled on the map (Figure 2.5.1-216) and the individual stream profiles.

On the Beaver Creek profile, an anomalously steep gradient is located directly south of Louisa and upstream from the up-dip projection of the rupture plane (Figures 2.5.1-216 and 2.5.1-217). This anomaly is located north of the Burton et al. (2014) map and west of the Marr (2002) and Mixon et al. (2000) maps. The anomaly is located within the Ellisville granodiorite and in close proximity to the northwest margin of the pluton

(1:500,000 scale state map of Dicken et al. 2005). The approximately 1,000-ft-long reach of steepened gradient (centered at approximately 33,000 ft in Figure 2.5.1-217) is likely not tectonic, since it is inconsistent with repeated deformation produced by a southeast-dipping reverse fault, such as the 2011 Mineral earthquake rupture. This feature also appears to be the anomalously steep gradient on Beaver Creek identified by Harrison (2012).

On the Harris Creek profile between horizontal distances of 11,000 and 17,000 feet in Figure 2.5.1-219, there is a slightly over-steepened reach of Harris Creek. This approximately 1-mile-long portion of the profile, which is slightly steeper than the adjacent reaches up and down stream, straddles the northwest margin of the Ellisville pluton tail (Figures 2.5.1-216 and 2.5.1-219) and does not cross any faults mapped by Burton et al. 2014 (Reference 2.5-396). The slightly oversteepened reach of the stream crosses five lithologies (from upstream to downstream) including Chopawamsic metafelsite (Ocf), Chopawamsic Fm undifferentiated (Oc), Chopawamsic metafelsite (Ocf), Chopawamsic quartzite and schist (Ocqs), and Ellisville granodiorite (Oeg). The latter two rock types (Ocqs and Oeg) exhibit very different landforms. The Chopawamsic quartzite and schist (purple unit on Figure 2.5.1-216) represents a relatively resistant unit and forms a series of linear ridges and topographic highs. The Ellisville granodiorite pluton tail is a less resistant lithology as evidenced by its spatial association with generally lower relief (Figure 2.5.1-212A) and lower elevations (Figure 2.5.1-212B). The subtle over-steepened reach of the stream is most likely lithologically controlled given the presence of such different rock types and their different expressions in the landscape.

Additional minor inflections or possible anomalies have been noted in the stream profiles, but are barely discernible at vertical exaggerations of twenty-five times (25x) and do not represent significant perturbations of the profiles. These have been noted on profiles of Beaver Creek, Contrary Creek, and South Anna River and are also summarized in Table 2.5.1-201. Those three very subtle features were highlighted in an attempt to recognize any potential anomaly, no matter how small or insignificant, in the epicentral area.

It is questionable if these subtle features actually represent any real inflection in the profiles at all, but have been included for completeness. The minor anomalies identified are extremely subtle features and most

likely represent very minor curvature in the profiles and not discrete inflections or true knickpoints. These features were identified as:

- Beaver Creek - a subtle inflection of gradient at a horizontal distance of about 20,000 ft and near the upward projection of rupture plane.
- Contrary Creek - a slightly steeper gradient in the uppermost 2,000 feet of profile.
- South Anna River - a subtle, broad inflection centered at a horizontal distance of about 30,000 to 40,000 ft (Figure 2.5.1-223) and near the upward projection of the rupture plane.

3. Other Geomorphic Studies

Following the Mineral earthquake, Berti et al. (2012) and Harrison (2012) identified geomorphic features that they interpreted as related to long-term surface deformation associated with tectonic processes in the epicentral area. In a conference abstract, Berti et al. (2012) note the presence of several geomorphic features that they describe as best explained by a history of tectonic uplift in the epicentral area:

- Several large knickpoints in the profile of the South Anna River, with one in particular that is about 1.5 miles northwest of project lidar coverage. This knickpoint lies almost directly on a fault contact between unit “OC?m” (Graywacke, phyllite, and melange) and unit “CZ?ss” (Metasandstone and phyllite) as mapped by Burton et al. (2014) (Reference 2.5-394). The upstream-side-up knickpoint has the opposite relationship expected from movement on a southeast-dipping reverse fault, and therefore likely does not reflect surface faulting.
- This knickpoint is described as accordant with a strath terrace that projects downstream to the epicentral area near Yanceyville. This location is not covered by project (or more recently available U.S. Geological Survey) lidar data. The terrace is further described as continuing several kilometers south of Yanceyville, gradually diverging upward from the South Anna River profile by approximately 6 m (20 ft). Due to the dramatic downstream increase in stream power and ability for the South Anna River to incise its channel, it is not unexpected that correlative terrace surfaces would lie at gradually increasing heights above the channel with distance downstream without tectonic influence.

- Lower sinuosity of the South Anna River to the north of the epicentral area, and higher sinuosity within the epicentral area. A qualitative visual assessment of the South Anna River from 10 m NED topographic data confirms an observable increase in sinuosity that begins near distance 45,000 ft on the South Anna River profile. Upstream of this point, river sinuosity is minimal. Downstream of this point, the sinuosity of the river increases and decreases non-systematically to its confluence with the North Anna River. The sinuosity of a stream has been shown to have a relationship with a number of processes, a concept summarized from multiple studies in Burbank and Anderson (2007) (Reference 2.5-395). These processes include the nature of the sediment load (e.g., grain size gradation, volume), stream velocity, stream power, and uplift. For the South Anna River, stream power dramatically increases at a point near the increase in sinuosity, which may imply a relationship. In any case, based on the variety of processes summarized by Burbank and Anderson (2007), stream sinuosity cannot be unequivocally attributed to surface deformation on the hanging wall of the Quail fault.

Also following the Mineral earthquake and in a conference abstract, Harrison (2012) identified two geomorphic features and describes them as suggestive of Quaternary tectonic activity:

- An anomalously steep reach of Beaver Creek. This stream anomaly, which is identified in map view (Figure 2.5.1-216) and the Beaver Creek profile (Figure 2.5.1-217) does not lie within the area of uncertainty of the up-dip projection of the rupture plane, nor does it correspond to the Harris Creek fault, Roundabout Farm fault, or other faults. This anomalously steep gradient lies within the Ellisville granodiorite and very close to the upstream contact with the Chopawamsic Formation based on regional, 1:500,000 scale mapping (Reference 2.5-245). While Harrison (2012) (Reference 2.5-401) states that this anomaly in Beaver Creek is suggestive of late Quaternary deformation, this has yet to be demonstrated. Alternatively, this stream anomaly may be related to the lithologic contrast along Ellisville granodiorite tail margin located directly upstream.
- A “Neogene alluvial terrace” located “directly over” the epicentral area described as terminated downstream by the “Sturgeon Creek/Freshwater Creek fault.” This relationship is described by

Harrison (2012) as suggestive of Quaternary deformation. The location of this terrace is not described in any greater detail by the author, and the Sturgeon Creek/Freshwater Creek fault is not shown on published maps within the epicentral area of the Mineral earthquake. Dominion's geologic field reconnaissance of the epicentral area did not find widespread alluvial terrace deposits, but locations of sparse lag gravels and gravel deposits on some of the higher ridges were found farther northeast, suggesting portions of the region may have once been blanketed by Tertiary-age fluvial gravel deposits, most of which have since been eroded away. Northeast of Lake Anna, Mixon et al.'s (2000) (SSAR Reference 44) geologic map of the 1:100,000 scale Fredericksburg sheet shows limited deposits of map unit Tms (Miocene sand and gravel). These deposits are distributed both northwest and southeast of northern projection of the Sturgeon Creek/Freshwater Creek fault, suggesting that this structure may not truncate the distribution of Tertiary gravels.

e. Conclusions

The following conclusions are based on the information provided above in this section:

- Seismologic data, as opposed to geologic data, provide the best definition of the rupture plane associated with the Mineral earthquake. Aftershocks and focal mechanism solutions for the Mineral earthquake define a rupture plane striking north-northeast to northeast (approximately 30-40°) and dipping moderately to the southeast (approximately 45-50°SE) (e.g., References 2.5-232, 2.5-235, and 2.5-392).
- The Mineral earthquake does not appear to have occurred on a previously mapped fault. It appears that the rupture plane defined by aftershocks lies structurally above (and east of) the Chopawamsic fault, and structurally below (and west of) the Long Branch fault. Thus, the source of the Mineral earthquake seems to be between these two southeast-dipping faults in the subsurface.
- Based on the field reconnaissance performed between April 19-21, 2012, no evidence of surface rupture, surface fault features, or geomorphic expression of surface rupture or coseismic surface tectonic deformation was recognized for the Mineral earthquake. Reconnaissance performed by the U.S. Geological Survey, the Virginia Division of Geology and Natural Resources, researchers from

Virginia Polytechnic Institute and State University, North Carolina State, and other academic institutions immediately following the earthquake concluded that the **M** 5.8 earthquake did not produce any discernible rupture or deformation at the ground surface.

- Geomorphic evaluations have not revealed definitive or strong evidence for the surface expression of the Mineral earthquake rupture plane or other neotectonic features. The landscape in the Mineral earthquake epicentral region appears to be strongly influenced by erosional differences between rock types, which is reflected by many topographic features (lineaments, drainages, and ridges) oriented parallel to geologic structural grain. In some cases, faults (e.g., Harris Creek fault) juxtapose different rock types and appear to be geomorphically expressed in high resolution lidar-derived imagery. The Harris Creek fault appears to exhibit greater geomorphic expression in areas where it juxtaposes different rock types and where it crosses the South Anna drainage. In areas where the Harris Creek fault separates similar rock types, however, the fault lacks geomorphic expression, suggesting the lithologic contrasts and proximity to the major trunk streams (higher rates of erosion) may be controlling subtle geomorphic lineaments. Within the stream profiles, only two prominent anomalies are recognized in the lidar within the 2011 Mineral earthquake epicentral region. The prominent anomaly on Harris Creek is coincident with the northwest margin of the Ellisville pluton tail and the other prominent anomaly on Beaver Creek is located very close to this same geologic contact and may also be lithologically controlled. Three additional very subtle gradient changes are also apparent in stream profiles. Since these can only be recognized when profiles are plotted at great vertical exaggerations (twenty-five to one hundred), these features are not considered meaningful geomorphic indicators of long term processes. While it is possible that some geomorphic features in the epicentral region could be related to neotectonic activity, there is no strong evidence to support this conclusion, and alternative and more compelling explanations exist.
- The moderate **M** 5.8 Mineral earthquake did not rupture the ground surface and it is unlikely that surface deformation (folding and uplift) associated with this single event would be readily discernible in the landscape. Unless the rate of tectonic deformation (recurrence

interval and displacement per event) on the causative fault of the Mineral earthquake greatly exceeds the erosion and denudation rates of the region, it may be very difficult to detect evidence for repeated Quaternary faulting and deformation in the landscape.

2.5.1.2.3 Site Area Stratigraphy

The third paragraph of this SSAR section is supplemented as follows with information that addresses the geological and geotechnical data collected from the additional Unit 3 borings.

NAPS COL 2.0-26-A

Seven borings were completed to depths ranging between 15 and 52 m (50 and 170 ft) during the ESP investigation (SSAR Appendix 2.5.4B). To supplement the existing geological and geotechnical data, 93 borings, 23 cone penetrometer tests (CPTs), 6 test pits, 5 sets of borehole geophysical logging, 5 sets of shear wave suspension logging, and 2 sets of electrical resistivity tests were performed as part of the subsurface investigation program for Unit 3. The boring data and geotechnical testing are discussed in detail in Section 2.5.4. The data developed by the Unit 3 subsurface investigation program are presented in Appendices 2.5.4AA, 2.5.4BB, and 2.5.4CC.

b. Ta River Metamorphic Suite (Cambrian and/or Ordovician)

The fourth paragraph of Item b of this SSAR section is supplemented as follows with information that summarizes the Unit 3 subsurface investigation program.

Borings completed during previous subsurface investigations at the NAPS site (SSAR References 7 and 8; and SSAR Appendix 2.5.4B) and borings completed as part of the Unit 3 subsurface investigation encountered rocks of the Ta River Metamorphic Suite at the Unit 3 site. (Appendices 2.5.4AA, 2.5.4BB, and 2.5.4CC)

Paragraphs six through ten of Item b of this SSAR section are supplemented as follows with information describing the results of the subsurface investigation performed for Unit 3.

NAPS ESP COL 2.5-1

Borings completed at the Unit 3 site as part of the Unit 3 subsurface investigation, documented in SSAR Reference 7, SSAR Appendix 2.5.4B, Appendices 2.5.4AA, 2.5.4BB, and 2.5.4CC, encountered the top of the moderately to highly weathered rock (Zone III)

from about Elevation 206 to 292 ft. The maximum thickness of the Zone III rock measured about 23.47 m (77 ft) and is described in the boring logs as a yellowish brown, gray, tan, reddish brown and dark green, very severely to moderately weathered, very closely to closely fractured, very soft to hard, biotite quartz gneiss and quartz biotite gneiss, with traces of clay, iron oxide staining, magnetite, muscovite and feldspar. In the central portion of the power block area, the Zone III rock is typically between elevations of about 260 to 280 ft. To true north and true south, this rock is typically at elevations of less than 240 ft. In three of the borings (M-11, B-917, and B-913) the top of the Zone III rock is at an elevation less than 220 ft. Of the three borings, the lowest recorded top of Zone III rock elevation is in boring B-917 at about 207 ft. The thickness of the saprolite overlying the Zone III rock is typically greatest at these boring locations, and in boring M-11 the combined thickness of Zones IIA and IIB saprolite reaches a maximum thickness of about 114 ft. The top of the slightly weathered to moderately weathered rock (Zone III-IV) was encountered in the borings at elevations ranging from about 187 to 292 feet and is generally described in the boring logs as a reddish brown to gray, moderately to slightly weathered, very close to moderately fractured, soft to very hard, biotite quartz gneiss and quartz biotite gneiss. The top of the slightly weathered to fresh rock (Zone IV) was encountered in the borings at elevations ranging between about 171 and 278 feet and is generally described in the boring logs as a gray and reddish brown, slightly weathered to fresh, very close to widely fractured, very hard, biotite quartz gneiss and quartz biotite gneiss. In the central portion of the power block area the top of Zone III-IV rock is typically between elevations of about 240 ft to 270 ft, with the exception of three borings (B-901, W-1, and B-903) where the top of Zone III-IV rock is at elevations of approximately 229 ft, 211 ft and 221 ft, respectively. To true north and true south, the top of the Zone III-IV rock is typically at an elevation less than 220 ft and a number of the borings exhibited an elevation less than 210 ft. The lowest recorded top of Zone III-IV rock elevation is in borings B-917 and W-9 at approximately 187 ft.

The last paragraph of Item b of this SSAR section is supplemented with a new paragraph on Unit 3-specific geologic boring results.

The borings exhibit severely weathered and jointed intervals in the Zone III-IV and Zone IV rock. These intervals were encountered in

several of the borings at varying elevations ranging from 150 ft to 285 ft. The intervals ranged in thickness from 0.2 to 20 ft (Appendices 2.5.4AA, 2.5.4BB, and 2.5.4CC). Characteristically, these intervals comprise poor to very poor quality rock that is highly fractured or jointed. The joints (typically sets of 3 to 10 joints) exhibit clay filling, iron and manganese oxide staining and occasionally quartz and feldspar veins. Occasionally, water loss in the fracture zones is reported to have occurred during drilling. Characteristically, these severely weathered zones are discolored or stained (except for quartz crystals), have a loss in rock strength, and contain some fragments of strong rock. On the boring logs these are usually heavily jointed, with occasional core loss noted. Based solely on weathering and elevation, there appears to be no way to confidently correlate weathered zones between borings. In boring W-1 a micro-shear zone in the Zone III-IV rock was encountered at an elevation of about 210 ft. It is described in the boring log as a possible shear zone, 0.6 ft thick comprising soft, yellow-brown clay with rock fragments. The apparent chloritized micro-shear zone at Elevation 210 ft in boring W-1 is a notable potential brittle shear zone. A 1.7 ft thick severely fractured clayey zone at Elevation 185.5 ft in boring W-5 is the one zone that most closely resembles the shear zone in boring W-1 because it also contains yellow-brown clay and chlorite. The micro shear zone in boring W-1 and the fractured clayey zone in boring W-5 do not appear to be correlated with fault "a". Both these borings plot along the 1:100,000 scale, Mixon et al. (2000), mapped trace of fault "a". However, the more accurate location of fault "a" is given by the detailed site mapping of trench and excavation exposures by Dames & Moore (1973) (SSAR Figure 2.5-18). Given that fault "a" dips approximately 45° to 50° to the northwest (Dames & Moore, 1973), borings W-1 and W-5 would encounter fault "a" at elevations much lower than these shear zones noted at Elevations of 210 ft and 185 ft, respectively. Therefore, these observed zones in the core samples do not represent fault "a". This apparent shear zone or zones in borings W-1 and W-5 appear to be isolated features and dissimilar to other discontinuities encountered in other borings. Quartz and feldspar veins encountered in the Zones III-IV and IV rock commonly contain traces of mica, garnet, magnetite, calcite, pyrite and occasional chlorite and epidote. These veins range in thickness from less than 0.1 ft to 0.8 ft. The thickest quartz vein at 0.8 ft thick encountered in boring M-1 is at an elevation of approximately 123 ft.

f. **Ellisville Pluton (Silurian)**

A new paragraph is added after the last paragraph of Item f of this SSAR section as follows.

Recent geologic mapping at a scale of 1:24,000 in the northern half of the Ferncliff, VA 7.5' quadrangle indicates that the Ellisville pluton appears to cross-cut and post-date the Chopawamsic thrust fault. This geologic mapping and age dating presented by Hughes and Hibbard (Reference 2.5-246) indicate that the Ellisville pluton (approximately 440 million years old) postdates thrusting and sinistral motion on the Chopawamsic fault (Section 2.5.3.2.1).

h. **Residual Soil and Saprolite (Cenozoic)**

Residual Soil

The second paragraph of Item h of this SSAR section is supplemented as follows with information to address residual soil characterization.

Residual soil was not encountered in any of the borings drilled as part of the Unit 3 subsurface investigation. (Appendices 2.5.4AA, 2.5.4BB, and 2.5.4CC)

Saprolite

Paragraph five of Item h of this SSAR section is supplemented as follows with a new paragraph that addresses geologic findings relative to saprolite.

Borings drilled as part of the subsurface investigation for Unit 3 encountered the top of the Zone IIA saprolite at elevations ranging from about 232 to 335 ft. The thickest Zone IIA saprolite encountered was about 28.65 m (94 ft) while the median thickness was about 9.14 m (30 ft). The saprolite is generally described in the boring logs as a yellowish red to yellowish brown to pale brown to greenish brown, medium dense to dense, clayey silt, silty sand and sand with relict rock fabric. The top of the Zone IIB saprolite was encountered at elevations ranging from about 215 to 302 ft. The thickest Zone IIB saprolite encountered was about 13.1 m (43 ft) while the median thickness was about 2.44 m (8 ft). The saprolite is generally described in the boring logs as a pale brown to reddish and yellowish brown to brownish gray to

greenish gray, very dense, fine to coarse grained sand and very severely weathered, soft to moderately hard gneiss with traces of clay, mafic minerals, and iron oxide staining.

k. **Artificial Material**

The first paragraph of Item k of this SSAR section is supplemented as follows with information to address findings relative to artificial material.

Borings performed as part of the subsurface investigation for Unit 3 encountered fill to depths of between about 0.12 to 5.48 m (0.4 and 18 ft) below the ground surface. The maximum thickness of fill (18 ft) was encountered in boring B-932 and is described in the boring log as a greenish gray and yellowish brown sandy silt and clay with traces of gravel and organic debris. Asphalt and road base, typically less than about one foot thick, was encountered in a number of borings (Appendices 2.5.4AA, 2.5.4BB, and 2.5.4CC).

The first paragraph of Item k of this SSAR section is supplemented with information on prohibiting the use of Zone IIA soil as structural fill.

NAPS ESP PC 3.E(5)

As described in Section 2.5.4.5.3, Zone IIA soil will not be used as structural fill to support Seismic Category I or II structures.

2.5.1.2.4 Site Area Structural Geology

The second sentence of the third paragraph of this SSAR section is replaced as follows.

NAPS ESP VAR 2.0-4

None of these faults are considered capable tectonic sources, as defined in RG 1.208, Appendix A.

2.5.1.2.6 Site Engineering Geology Evaluation

a. **Engineering Behavior of Soil and Rock**

Soil

The second paragraph under Soil in Item a of this SSAR section is supplemented as follows with information to address soil behavior.

NAPS COL 2.0-26-A

The saprolite at the Unit 3 site has been categorized into Zone IIA and Zone IIB saprolite, based on its general composition and grain size (Section 2.5.4). Grain size tests on samples of the Zone IIA saprolite

show that the median fines content for the saprolite is about 24 percent with the majority of the samples classified as a silty sand (SM). Grain size tests on samples of the Zone IIB saprolite show that the fines content for the saprolite ranges from about 15 to 27 percent. The saprolite is also classified as a silty sand (SM). Zone IIA saprolite is the more weathered of the two saprolites and contains less than 10 percent rock fragments with relict texture. The borings drilled as part of the subsurface investigation for Unit 3, documented in Appendices 2.5.4AA, 2.5.4BB, and 2.5.4CC, reveal that SPT N-values ranged from 2 to refusal, with a median value of 15 blows per foot (bpf) for this saprolite. Zone IIB saprolite contains between 10 and 50 percent relict rock fragments, and SPT N-values ranged from 24 to refusal with a median value of 75 bpf. Section 2.5.4 contains a detailed discussion of the geotechnical properties of the saprolite at the Unit 3 site.

Rock

The second paragraph under Rock of Item a of this SSAR section is supplemented as follows with information to address rock behavior.

Based on the results of the borings drilled as part of the subsurface investigation for Unit 3, documented in Appendix 2.5.4AA, rock quality designation (RQD) generally ranges from zero to 50 percent for the Zone III rock with an average RQD value of about 20 percent. An RQD of 20 percent is indicative of very poor quality rock (SSAR Reference 109).

The third paragraph under Rock of Item a of this SSAR section is supplemented as follows with information to address rock behavior.

Based on the results of the borings drilled as part of the subsurface investigation for Unit 3 and documented in Appendices 2.5.4AA, 2.5.4BB, and 2.5.4CC, RQD generally ranges from about 50 to 90 percent for the Zone III-IV rock with an average value of about 65 percent, indicative of fair quality rock (SSAR Reference 109). For the Zone IV rock, RQD is generally above 80 percent and mostly above 90 percent. The average RQD value is 95 percent, indicative of excellent quality rock (SSAR Reference 109). The boring results for the previous geotechnical investigations (SSAR References 7 and 8), and for both the ESP subsurface investigation (Reference 2.5-201) and the Unit 3 subsurface investigation (Appendices 2.5.4AA, 2.5.4BB, and 2.5.4CC)

indicate that Zones III, III-IV and IV are suitable bearing surfaces on which to found the Seismic Category I structures. The RB, Fuel Building, and the Control Building, will be founded on the Zone III-IV or Zone IV bedrock; where the top of this bedrock is below the foundation level, the overlying materials will be replaced with concrete fill. The FWSC will be founded on Zone III rock or on concrete fill above the top of the Zone III rock. The joints and fractures present in these zones are not of sufficient density or areal extent to affect the engineering behavior of the rock with respect to its foundation bearing capacity or integrity.

b. **Zones of Alteration, Weathering and Structural Weakness**

The third paragraph of Item b of this SSAR section is supplemented as follows with information to address zones of alteration, weathering and structural weakness.

Borings completed as part of the ESP subsurface investigation program (SSAR Appendix 2.5.4B) and the Unit 3 COL subsurface investigation programs (Appendices 2.5.4AA, 2.5.4BB, and 2.5.4CC) reveal zones of severely weathered and fractured rock in the moderately to slightly weathered (Zone III-IV) and slightly weathered to fresh rock (Zone IV). The zones are at elevations ranging between about 150 ft and 285 ft and range in thickness from 0.2 ft to 20 ft with a median thickness of about 5 ft. RQD values in these zones range from 0 to 40 percent with a median value of about 10 percent. Characteristically, these fracture zones exhibit clay filling, iron and manganese oxide staining and, occasionally, quartz and feldspar veins. Occasionally, water loss in the fracture zones is reported to have occurred during drilling.

The fourth paragraph of Item b of this SSAR section is supplemented as follows with information on excavation and replacement of weathered or fractured rock.

NAPS ESP PC 3.E(4)

Weathered or fractured rock at the foundation level for safety-related structures will be excavated and replaced with lean concrete before initiation of foundation construction. See also Section 2.5.4.10.

d. **Prior Earthquake Effects**

The last sentence of the second paragraph of Item d of this SSAR section is replaced as follows.

NAPS ESP VAR 2.0-4

The Unit 3 site is located within the CVSZ, which is an area of persistent, low-level seismicity in the Piedmont Province and ECC-AM source zone, as described in Section 2.5.1.1.4.d.1. (Reference 2.5-223)

f. **Construction Groundwater Control**

The first paragraph of Item f of this SSAR section is supplemented as follows with information to address ground water level.

Groundwater levels at the site are expected to result in the need for temporary dewatering of foundation excavations extending below the water table. Dewatering will be performed in a manner that minimizes drawdown effects on the surrounding environment. Drawdown effects will be limited to the Unit 3 site and no offsite users will be affected.

g. **Unforeseen Geologic Features**

The first paragraph of Item g of this SSAR section is supplemented as follows with information to address geologic mapping of excavations of safety-related structures.

NAPS ESP PC 3.E(6)

Future excavations for safety-related structures will be geologically mapped. Unforeseen geologic features that are encountered will be evaluated. The NRC will be notified no later than 30 days before any excavations for safety-related structures are open for NRC examination and evaluation. See also Section 2.5.4.5.2.

2.5.1.2.7 Site Groundwater Conditions

The second paragraph of this SSAR section is supplemented as follows with information to address site groundwater conditions.

NAPS COL 2.0-26-A

A detailed discussion of Unit 3 site groundwater conditions based on the Unit 3 subsurface investigation is provided in Section 2.4.12.

NAPS COL 2.0-26-A

Table 2.5.1-201 **Summary of Stream Profile Assessments**

Profile Name[1]	Anomaly	Location[2]	Spatially coincident with lithologic change?	Comments
Beaver Creek	*Prominent* anomalously steep gradient	Approx. 33,000 ft	Possibly	• Prominent feature that can be recognized in profile with vertical exaggeration of only ten (10x). • Over-steepened reach of stream is about 1,000 ft long. • Detailed geologic mapping not available for this location. On the 1:500,000 scale state geologic map, this steeper portion of the stream lies within the Ellisville granodiorite and directly downstream of the pluton/Chopawamsic Formation contact.
Beaver Creek	*Very subtle* change in gradient	Approx. 20,000 ft	No	• Very subtle feature that can only be seen at significant vertical exaggeration of profile (25x and greater). • Gradient change is gradual and not a discrete point of inflection. Broad convex-upward curvature in profile is centered at about 20,000 ft. • Center of gradient change (at approx. 20,000 ft) lies within Ellisville granodiorite near the unnamed north strand of the Harris Creek fault and within the area of uncertainty for up-dip projection of aftershock plane.
Contrary Creek	Subtle steeper gradient	0 to 2,000 ft	Yes	• Upper roughly 2,000 feet of headwaters is steepened. • Steepened reach is coincident with the rocks of the Mine Run Complex II and downstream inflection is coincident with the Chopawamsic Fm contact (based geologic map of Mixon et al. (2000)) and steeper gradient in headwaters.
Harris Creek	*Prominent* steep gradient	Approx. 11,000 to 17,000 ft	Yes	• Steep gradient is easily recognized at vertical exaggeration of 25x. • Length of stream exhibiting steeper gradient is approximately 6,000 ft. • Over-steepened reach of stream begins in the Chopawamsic Fm upstream and ends in the Ellisville granodiorite downstream. Various rocks of the Chopawamsic Formation include the resistant unit of quartzite and schist that forms linear ridges across the landscape. • Steep reach of stream lies directly upstream of area of uncertainty for up-dip projection of aftershock plane.

NAPS COL 2.0-26-A

Table 2.5.1-201 **Summary of Stream Profile Assessments** *(continued)*

Profile Name[1]	Anomaly	Location[2]	Spatially coincident with lithologic change?	Comments
Northeast Creek	None	NA	NA	No apparent anomalies.
Roundabout Creek	None	NA	NA	No apparent anomalies.
South Anna River	*Very* subtle change in gradient	Approx. 30,000 to 40,000 ft	Yes	• Very subtle feature recognized only at significant vertical exaggerations of profile (100x) but not discernible at vertical exaggeration of 25x. • Gradient change is gradual and not a discrete point of inflection and may represent a broad concave-upward curvature in profile. • Feature lies within area of uncertainty for up-dip projection of aftershock plane. • Subtle gradient change reflects slightly steeper gradient upstream and shallower downstream. This geometry is opposite of what would be expected from repeated slip on a southeast dipping reverse fault. • Subtle feature is approximately centered near the southeast margin of the Ellisville granodiorite pluton tail.

Notes:

1. All profiles cross 2011 Mineral earthquake rupture plane except the Contrary Creek profile.
2. Based on approximate horizontal stationing (in feet) along x-axis of profile figure.

NAPS COL 2.0-26-A Figure 2.5.1-201 **Lidar Survey Location Map**

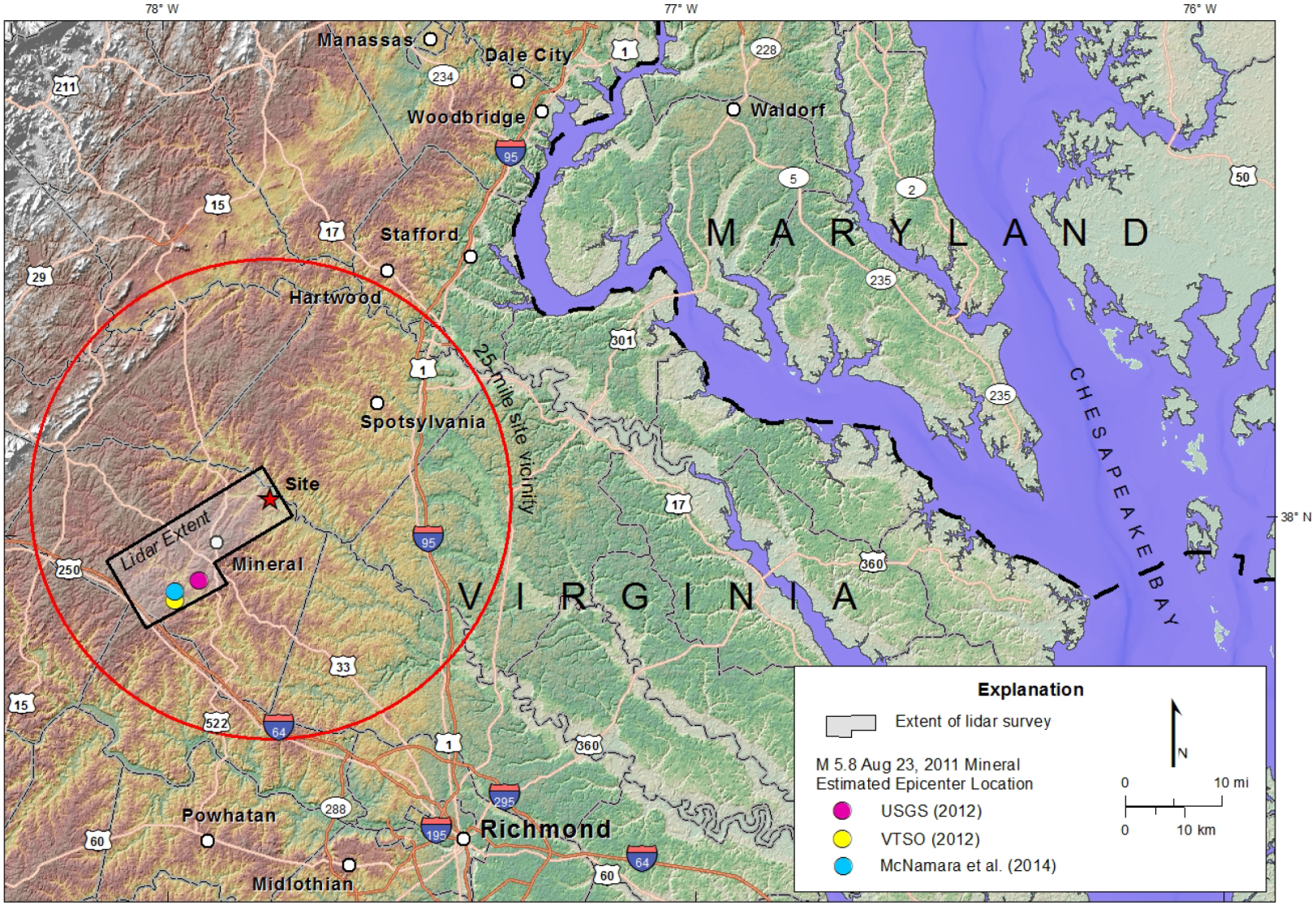

NAPS COL 2.0-26-A Figure 2.5.1-202 **CEUS SSC Sources Zones**

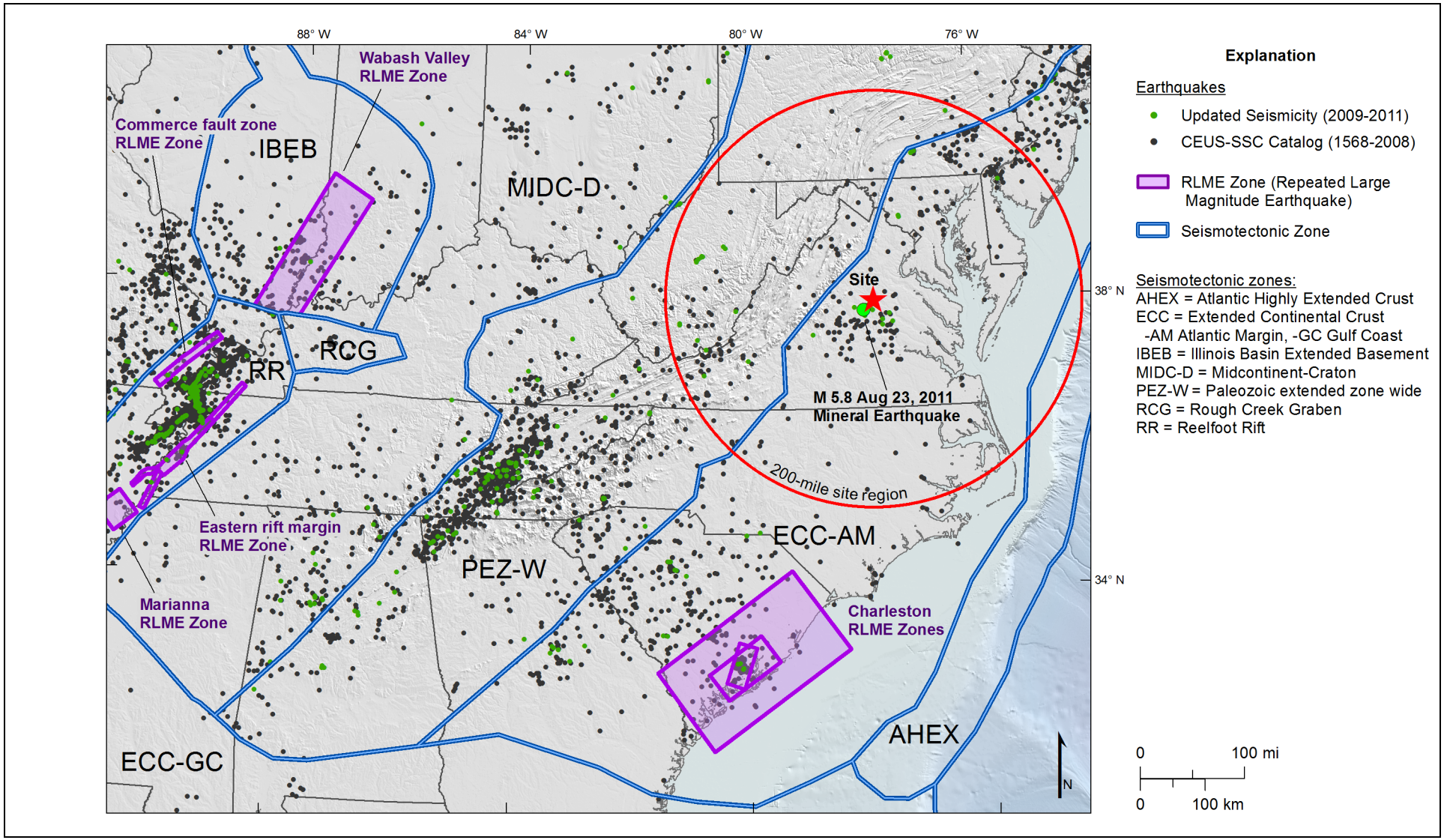

NAPS COL 2.0-26-A Figure 2.5.1-203(A), (B), and (C) **Mineral Earthquake Hypocentral Data**

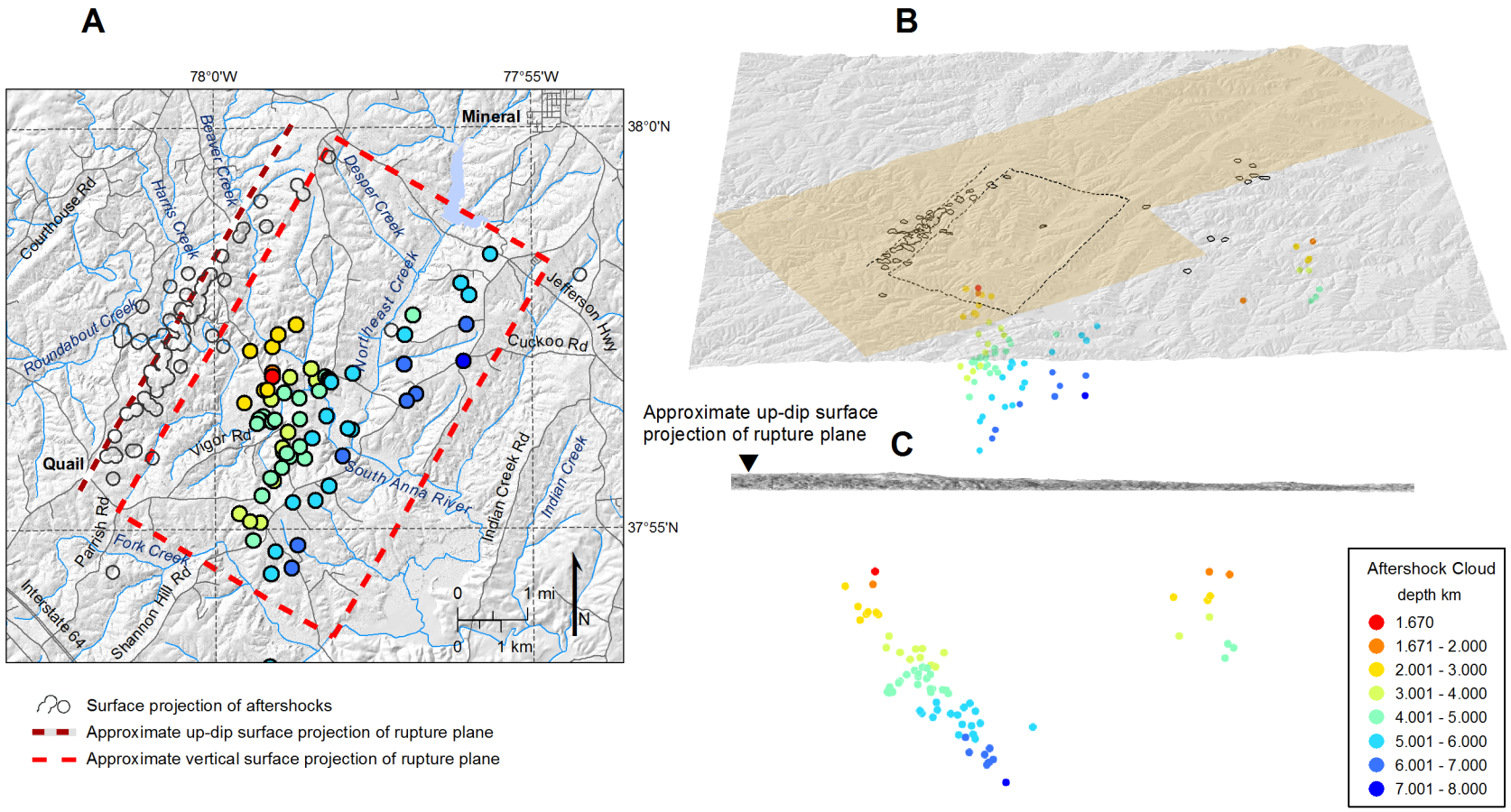

Notes:

1. Map of approximate vertical projection (dashed rectangle) of rupture plane estimated from August 25–September 1, 2011 aftershocks (Reference 2.5-242) and approximate up-dip surface projection of rupture plane (dashed line) based on surface projected aftershocks. These surface-projected aftershocks define the area where fault would intersect the ground surface.
2. 3-dimensional perspective view of aftershocks defining the rupture plane (view to the north).
3. Aftershocks defining eastward dip of fault (view N30E along strike of rupture).

NAPS COL 2.0-26-A Figure 2.5.1-204 **Field Reconnaissance Routes and Waypoints**

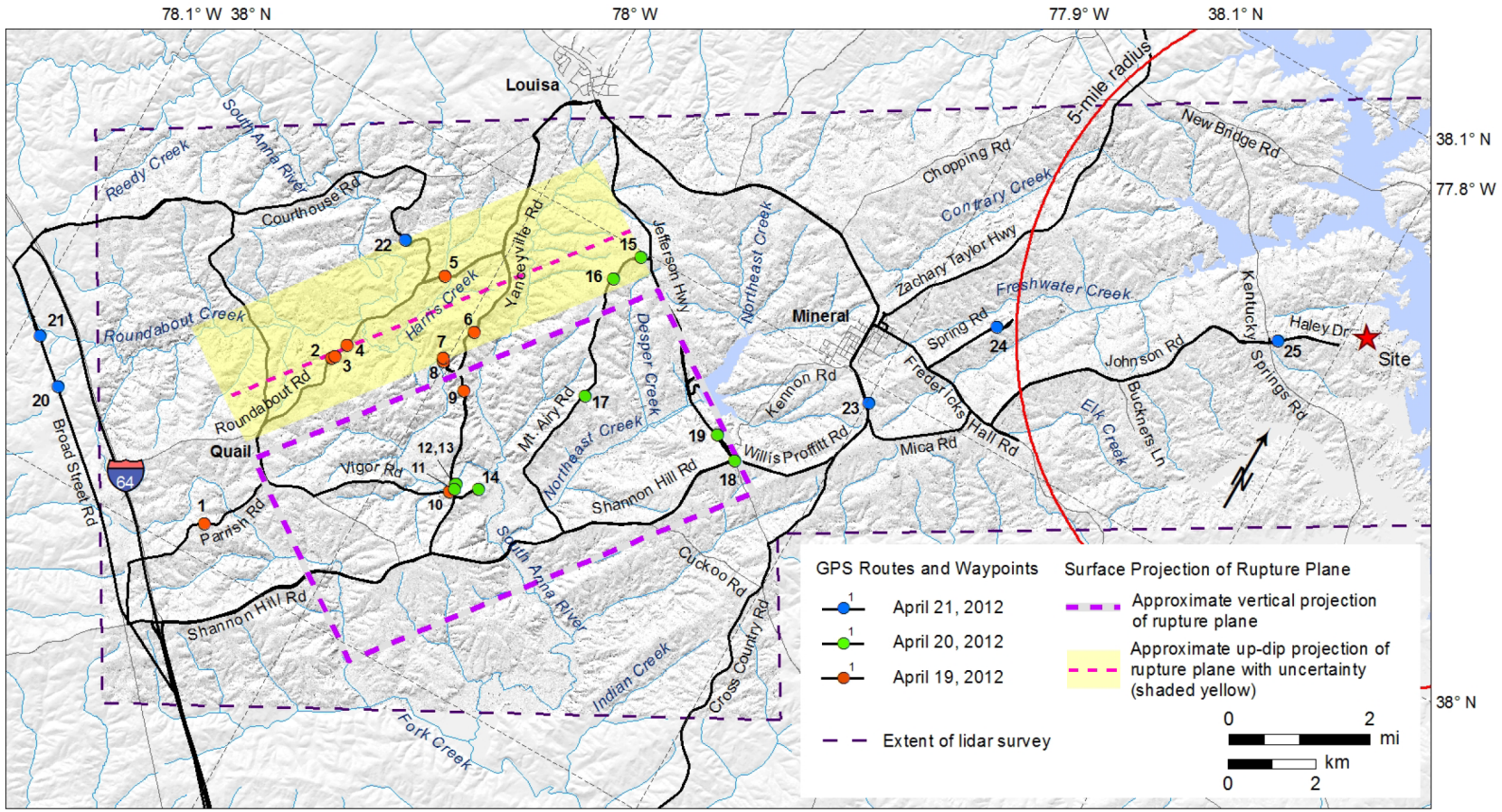

Note: Approximate vertical and up-dip surface projections of the Mineral earthquake aftershock plane based on data from McNamara et al. (2014) (Reference 2.5-392).

NAPS COL 2.0-26-A Figure 2.5.1-205 **Geologic Map of the Mineral Earthquake Study Area (1:500,000 scale)**

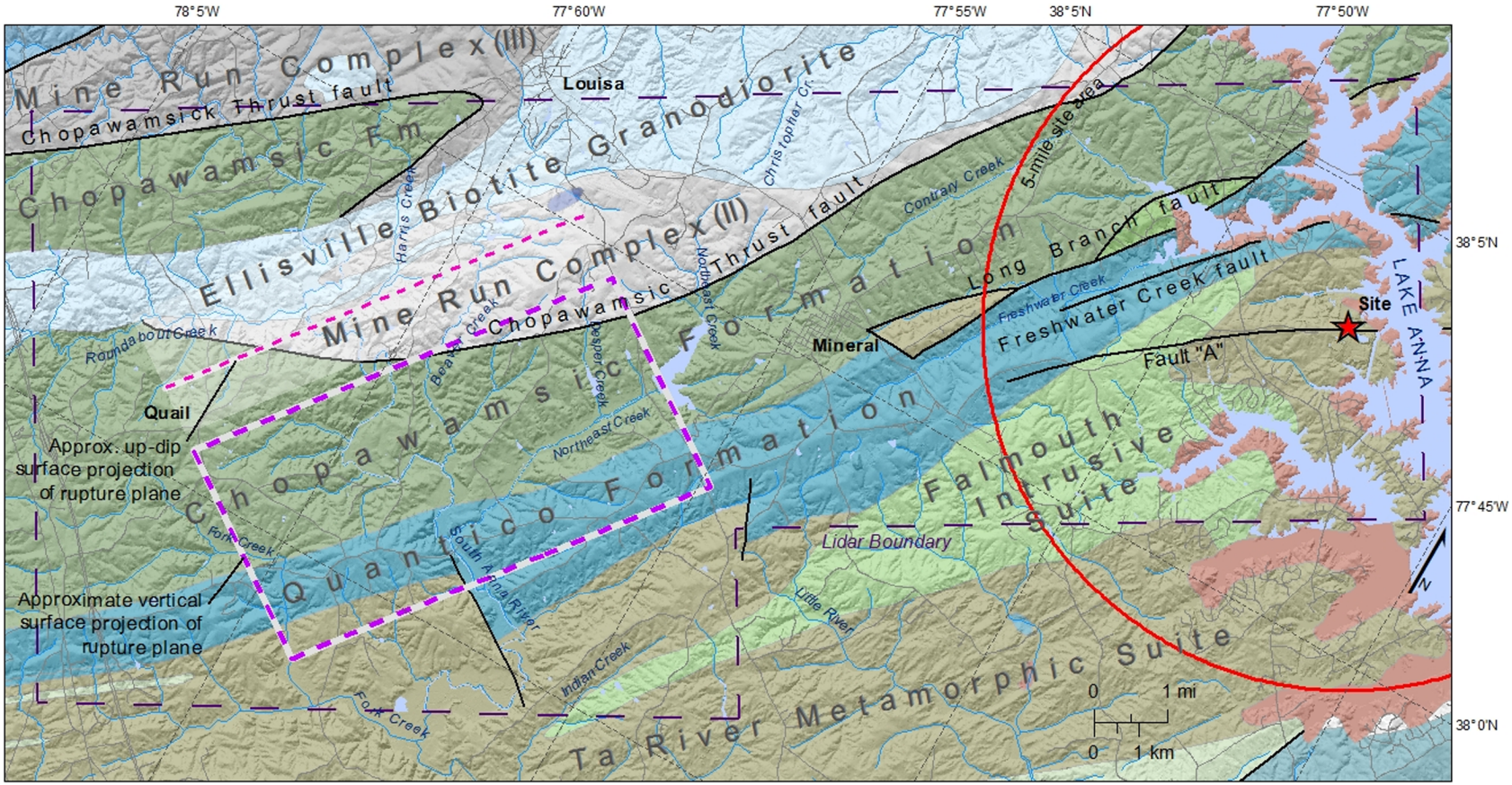

Note: Approximate vertical (purple dashed polygon) and up-dip surface (red dashed line) projections of the Mineral earthquake aftershock plane based on data from McNamara et al. (2014) (Reference 2.5-392).

NAPS COL 2.0-26-A Figure 2.5.1-206 **Geologic Compilation Map with Numbered GPS Waypoint Locations**

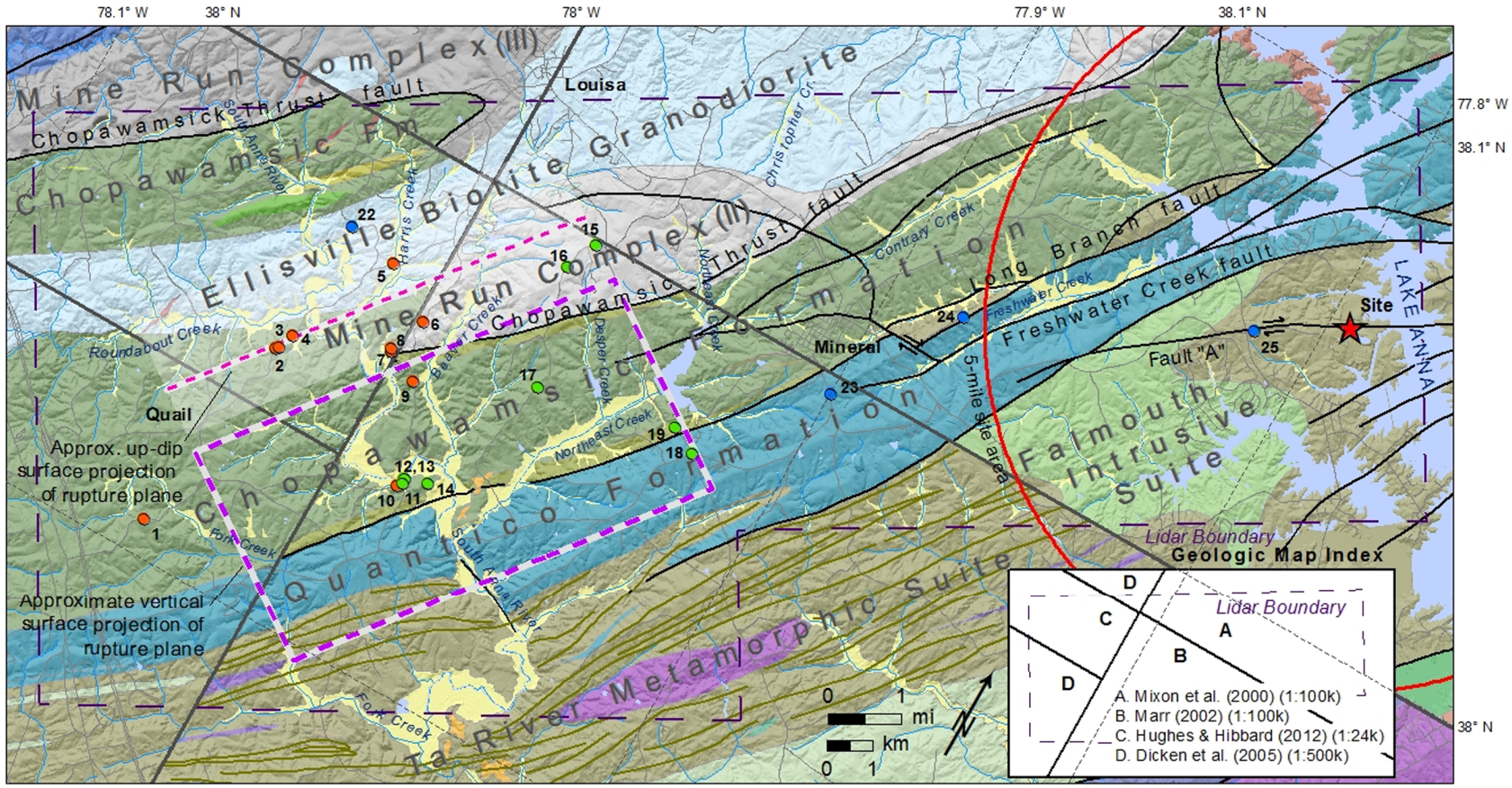

Notes:

1. Mismatches in geologic units at map boundaries.
2. Faults shown as thin black lines.
3. Low relief associated with Ellisville biotite granodiorite pluton.
4. Contact area is from 1:500,000-scale geologic map.
5. Approximate vertical (purple dashed polygon) and up-dip surface (red dashed line) projections of the Mineral earthquake aftershock plane based on data from McNamara et al. (2014) (Reference 2.5-392). Numbered circles indicate field reconnaissance waypoints.

NAPS COL 2.0-26-A Figure 2.5.1-207 **Color-Shaded Relief Map**

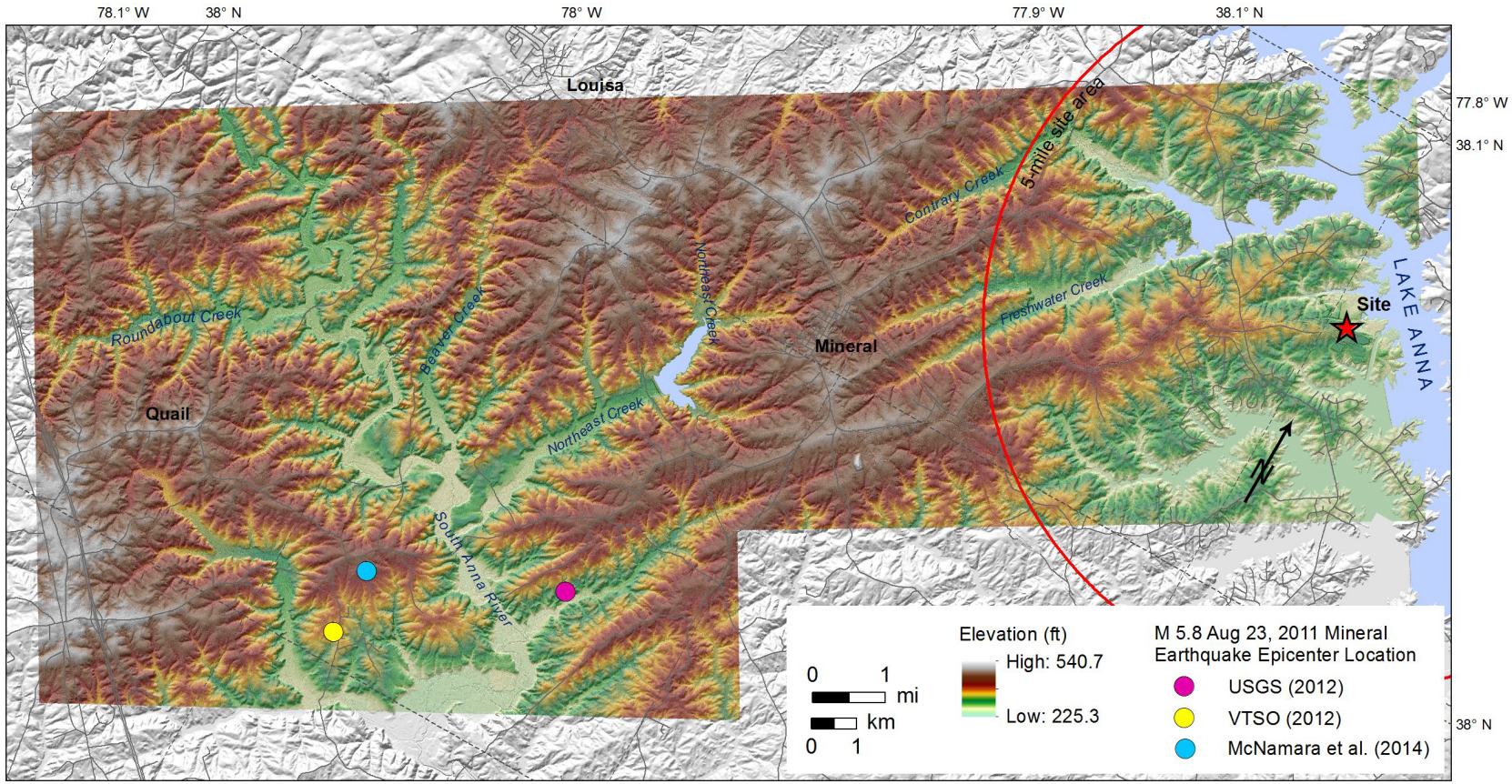

NAPS COL 2.0-26-A Figure 2.5.1-208 **Mineral Earthquake Aftershock Data**

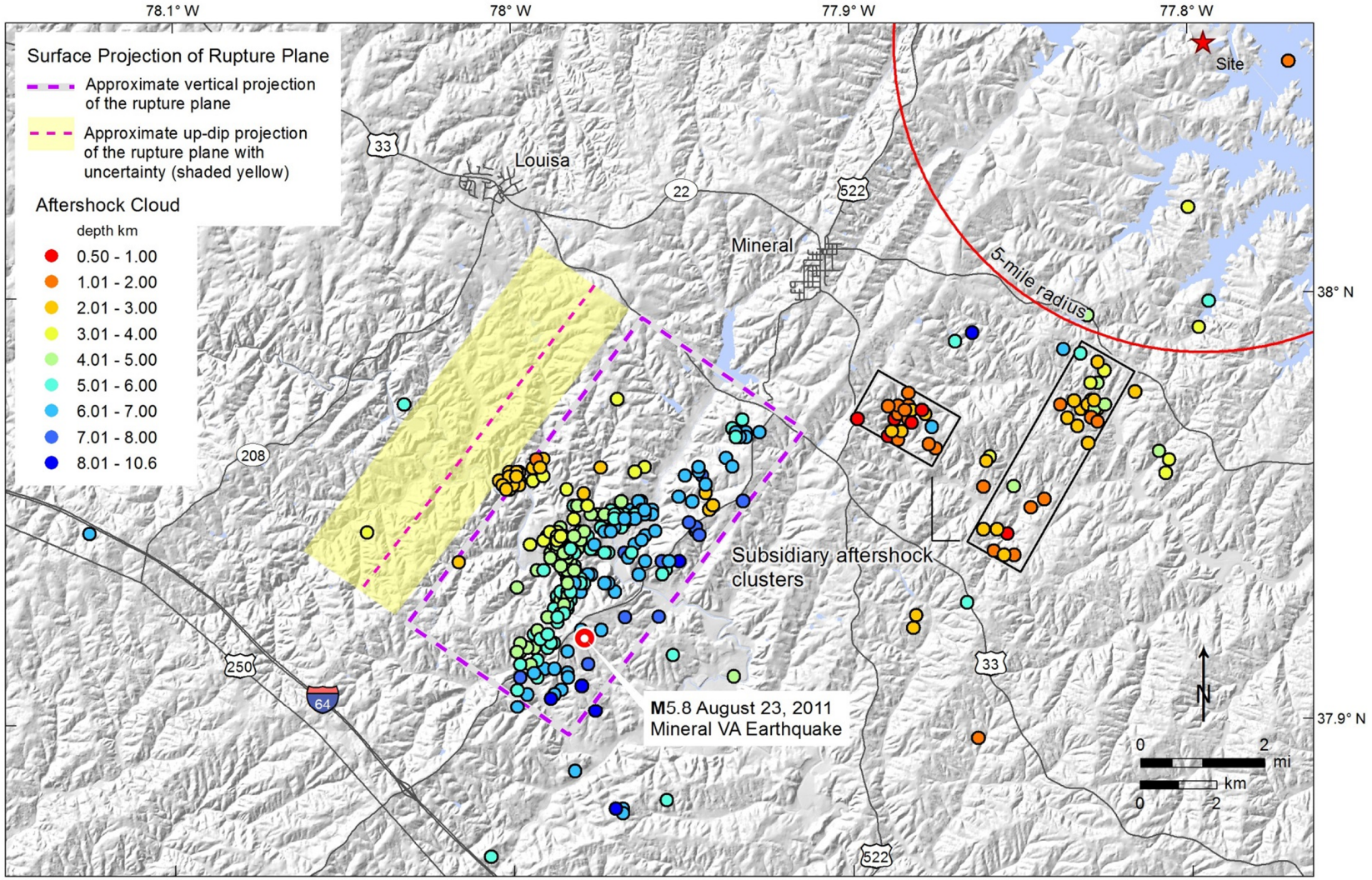

Note: Data from McNamara et al. (2014) (Reference 2.5-392)

Figure 2.5.1-209 **Mineral Earthquake Aftershock Cross-Sections**

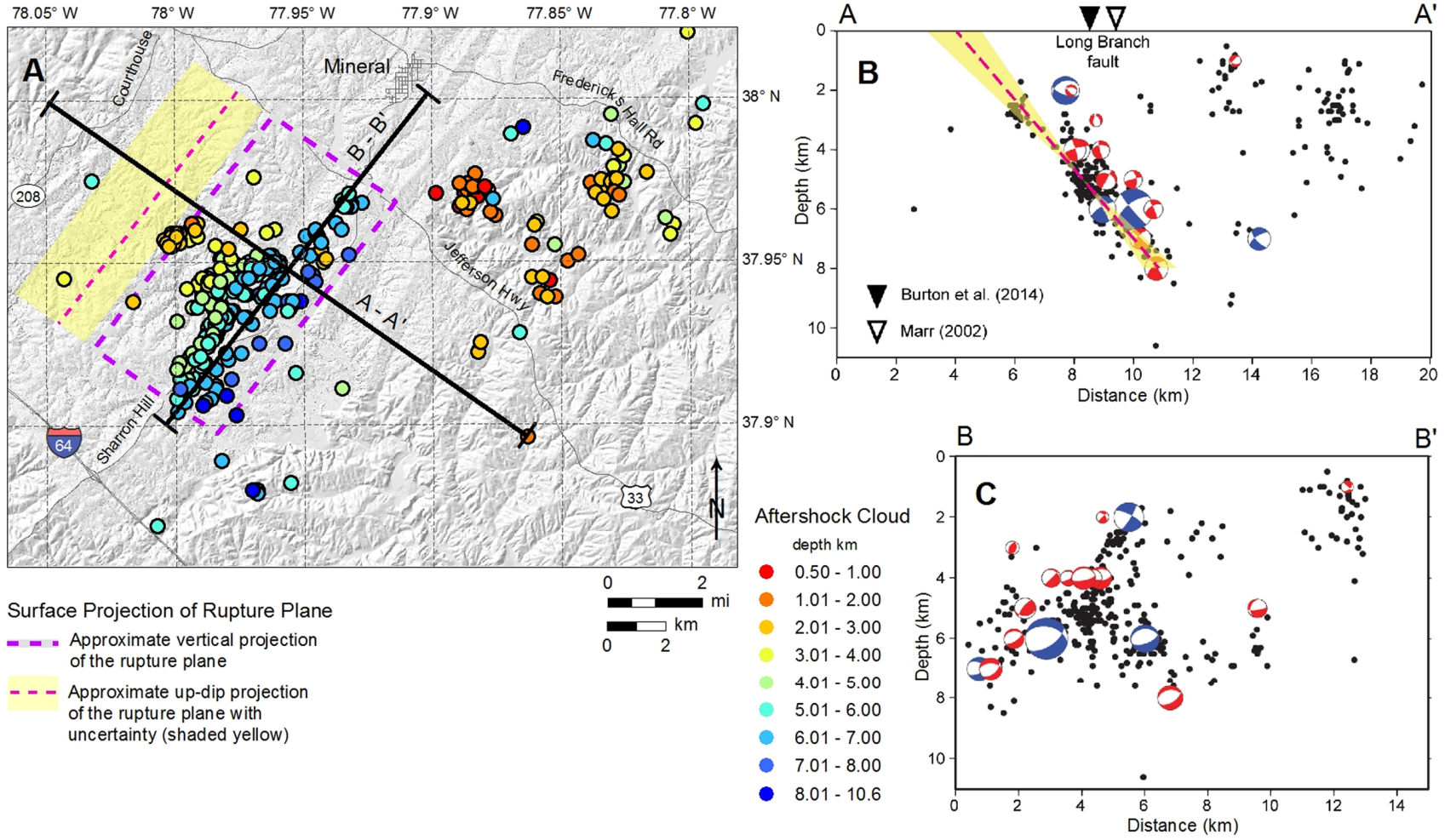

Note: Modified from McNamara et al. (2014) (Reference 2.5-392)